

Validation of GEMS tropospheric NO₂ columns and their diurnal variation with ground-based DOAS measurements

Kezia Lange¹, Andreas Richter¹, Tim Bösch¹, Bianca Zilker¹, Miriam Latsch¹, Lisa K. Behrens¹, Chisom M. Okafor¹, Hartmut Bösch¹, John P. Burrows¹, Alexis Merlaud², Gaia Pinardi², Caroline Fayt², Martina M. Friedrich², Ermioni Dimitropoulou², Michel Van Roozendael², Steffen Ziegler³, Simona Ripperger-Lukosiunaite³, Leon Kuhn³, Bianca Lauster³, Thomas Wagner³, Hyunkee Hong⁴, Donghee Kim⁴, Lim-Seok Chang⁴, Kangho Bae^{5,6}, Chang-Keun Song^{5,6,7}, Jong-Uk Park⁸, and Hanlim Lee⁹

¹Institute of Environmental Physics, University of Bremen, Bremen, Germany

²Royal Belgian Institute for Space Aeronomy, Brussels, Belgium

³Max Planck Institute for Chemistry, Mainz, Germany

⁴Environmental Satellite Center, National Institute of Environmental Research, Incheon, Republic of Korea

⁵Department of Civil, Urban, Earth and Environmental Engineering, Ulsan National Institute of Science and Technology, Ulsan, Republic of Korea

⁶Research & Management Center for Particulate Matters at the Southeast Region of Korea, Ulsan National Institute of Science and Technology, Ulsan, Republic of Korea

⁷School of Carbon Neutrality, Ulsan National Institute of Science and Technology, Ulsan, Republic of Korea

⁸School of Earth and Environmental Sciences, Seoul National University, Seoul, Republic of Korea

⁹Division of Earth Environmental System Science, Major of Spatial Information Engineering, Pukyong National University, Busan, Republic of Korea

Correspondence: Kezia Lange (klange@iup.physik.uni-bremen.de)

Abstract. Instruments for air quality observations on geostationary satellites provide multiple observations per day and allow for the analysis of the diurnal variation of important air pollutants such as nitrogen dioxide (NO₂) ~~over large areas~~. The South Korean instrument GEMS ~~on the GK2B satellite was~~ launched in February 2020 ~~and~~ is the first ~~instrument in geostationary orbit that delivers hourly daytime observations~~ geostationary instrument that is able to observe the diurnal variation of NO₂.

5 The measurements with have a spatial resolution of 3.5 km × 8 km, and cover a large part of Asia.

This study compares one year of tropospheric NO₂ vertical column density (VCD) observations ~~of from~~ the operational GEMS L2 product, the scientific GEMS IUP-UB product, the operational TROPOMI product, and ground-based DOAS measurements in South Korea. The GEMS L2 tropospheric NO₂ VCDs overestimate the ~~VCDs retrieved from the ground-based observations~~ tropospheric NO₂ VCDs with a median relative difference of +64.61 % and a correlation coefficient of 0.750.76. The median

10 relative difference is -1.2 % for the GEMS IUP-UB product and -14.16 % for the TROPOMI product. ~~The evaluation of the GEMS IUP-UB product and the operational TROPOMI product with ground-based measurements is in good agreement with~~ with correlation coefficients of 0.82 and 0.880.83 and 0.89 respectively. The scatter in the GEMS products can be reduced when observations are limited to the TROPOMI overpass time.

~~The observed diurnal variations of the~~ Diurnal variations of tropospheric NO₂ VCDs ~~show a maximum of NO₂ during the late morning for urban sites, whereas rural sites differ by pollution level of the analyzed site but with good agreement between the~~

GEMS IUP-UB and ground-based observations. Low polluted sites show weak or almost no diurnal ~~changes.~~ Investigations of the seasonal diurnal variability show with a minimum in the observed tropospheric NO₂ VCDs around noon the importance of chemical loss of NO₂ in summer. Most variability variation. In summer, the polluted sites show a minimum around noon, indicating the large influence of photochemical loss. Most variation is seen in spring and autumn, ~~which dominate the average annual diurnal cycle.~~ Observations with increasing NO₂ in the morning, a maximum close to noon, and a decrease towards the afternoon. Winter observations show rather flat or slightly decreasing NO₂ over the day. Winter observations under low wind conditions ~~show strong at high polluted sites show~~ enhancements of NO₂ over the day, ~~especially at polluted sites during winter.~~ This indicates that under calm conditions, dilution and the less effective chemical loss in winter do not balance the accumulating emissions. ~~The impact of transport processes is illustrated by the diurnal variability at a rural site following mean wind patterns for specific seasons and observation times~~ Diurnal variation observed at a low polluted site follows seasonal wind patterns.

~~Analyzing the weekday-weekend effect, good agreement was found.~~ Weekday-weekend effect analysis shows good agreement between the different products. However, the GEMS L2 product while agreeing with the other data sets during weekdays shows significantly less reduction on weekends.

~~Our investigations show that the observed diurnal evolution of~~ The influence of the stratospheric contribution and the surface reflectivity product on the satellite tropospheric NO₂ varies significantly at the different measurement sites, with good agreement between the GEMS IUP-UB and ground-based observations. The diurnal variability of VCD products are investigated. While the TM5 model's stratospheric VCDs, used in the TROPOMI product, are too high, resulting in too low and even negative tropospheric NO₂ VCDs depends on chemistry, emissions, and transport into and out of the measurement region. To interpret the sources and sinks of NO₂ requires that all of these factors are considered., when used in the GEMS IUP-UB retrieval, the GEMS L2 stratospheric VCD is too low. Surface reflectivity comparisons indicate that the GEMS L2 reflectivity has a large contribution to the observed overestimation and scatter.

1 Introduction

Nitrogen oxides, in particular nitrogen monoxide (NO) and nitrogen dioxide (NO₂), collectively referred to as NO_x, are among the most important air pollutants and strongly impact tropospheric chemistry. NO_x is emitted into the atmosphere by natural sources such as lightning and soil microbial processes, but the primary source is anthropogenic activities. Anthropogenic emissions ~~are caused by~~ result from fossil fuel combustion mainly for transportation, the industry and energy ~~sector~~ sectors, and residential heating (Seinfeld and Pandis, 2006; Wallace and Hobbs, 2006). High concentrations of NO_x are a health hazard ; ~~which gets especially relevant as~~ and of growing importance for environmental legislation, since most anthropogenic sources are concentrated in urban areas with high population densities ~~Faustini et al. (2014)~~ (Faustini et al., 2014).

Tropospheric NO_x is mainly emitted as NO, which is rapidly converted to NO₂ by the reaction with tropospheric ozone (O₃). Due to their short atmospheric lifetimes, on the order of a few hours in the boundary layer during daytime (Beirle et al., 2011), the heterogeneous distribution of sources and variations of meteorological conditions, tropospheric NO₂ shows high spatial

and temporal variability. Monitoring and understanding this variability is necessary to better understand the contributions of emissions, tropospheric chemistry, and transport effects, especially in urban areas with large and heterogeneous NO_x sources combined with high population densities.

To resolve this spatial and temporal variation of tropospheric NO_2 , measurements with good spatial and temporal resolution are needed. NO_2 can be remotely observed using the DOAS (differential optical absorption spectroscopy) technique (Platt and Perner, 1980). DOAS measurements of NO_2 have been performed from different platforms, including ground-based stations, moving platforms such as cars, ships, or aircraft, and environmental satellites, with advantages and disadvantages regarding spatial and temporal resolution.

Stationary ground-based instruments such as multi axis DOAS (MAX-DOAS, ~~(see e.g., Hönninger et al., 2004; Wittrock et al., 2004; Herman et al., 2009)~~ can see e.g., Hönninger et al. (2004); Wittrock et al. (2004); Herman et al. (2009)) provide several observations of NO_2 column densities per hour ~~but are limited to their at a given~~ location. These data sets are commonly continuous and are valuable for the validation of satellite ~~observations~~data products, among other applications (e.g., Pinaridi et al., 2020; Verhoelst et al., 2021).

Mobile car DOAS measurements enable the observation of ~~spatial variability~~the spatial distribution in addition to its temporal evolution and are an additional valuable source for ~~satellite validation~~the validation of satellite trace gas data products (e.g., Wagner et al., 2010). They fill a gap between stationary ground-based and satellite observations by mapping the variability within ~~satellite pixels~~the satellite pixel and quantifying errors for satellite and stationary ground-based comparisons.

The advantage of measurements from environmental satellites in polar sun-synchronous low earth orbit (LEO) is that they can provide global coverage. The spatial resolution of satellite observations making use of the DOAS method has increased strongly since the first mission with a ground footprint of $320 \text{ km} \times 40 \text{ km}$ for the Global Ozone Monitoring Experiment (GOME) in 1995 (Burrows et al., 1999) to the recent TROPOspheric Monitoring Instrument (TROPOMI) with a spatial resolution of $5.5 \text{ km} \times 3.5 \text{ km}$ (Veefkind et al., 2012). ~~This TROPOMI measurements~~ offers the possibility to deconvolve sources of NO_x , such as individual power plants, and to quantify their emissions (~~Beirle et al., 2019a~~)(e.g., Beirle et al., 2019a). Satellite measurements also enable the seasonal variations of NO_2 to be observed globally. This has been done, for example, using SCIAMACHY (Bovensmann et al., 1999) observations to disentangle the sources of NO_x (van der A et al., 2008) or using TROPOMI observations to analyze the seasonality of NO_x emissions and lifetimes (Lorente et al., 2019; Lange et al., 2022).

~~However, instruments~~Instruments in low earth orbits usually provide at best only one measurement per day and ~~per location~~location in low and mid latitudes. Combining observations from several satellites with different overpass times provides some ~~additional information on~~information about the diurnal variation of NO_2 . Several studies have applied this method, based on the morning overpasses of the SCIAMACHY or GOME-2 (Munro et al., 2006) instrument and the early afternoon observation of the Ozone Monitoring Instrument (OMI, Levelt et al. (2006))~~(see e.g., Boersma et al., 2008, 2009; Penn and Holloway, 2020)~~ ~~-, see e.g., Boersma et al. (2008, 2009); Penn and Holloway (2020)~~. Boersma et al. (2008) used SCIAMACHY and OMI ~~data~~observations to estimate the diurnal ~~variability~~variation of NO_2 . Over urban regions, they found up to 40 % reduced NO_2 columns in the OMI afternoon overpass compared to the SCIAMACHY morning overpass. They explained this by photochemical loss, ~~dampened~~modulated by the diurnal cycle of anthropogenic emissions. Over biomass burning regions, they detected

an increase from the morning to the afternoon overpass, which is consistent with fire counts from the geostationary satellites.

85 Analyzing the differences between SCIAMACHY and OMI tropospheric NO₂ columns from Israeli cities, Boersma et al. (2009) found again 40 % reduction for NO₂ columns in the afternoon compared to the morning overpass during summer, and nearly no differences in winter with only slightly higher NO₂ in the afternoon. Penn and Holloway (2020) found around 1.5–2 times higher NO₂ columns for the morning compared to the afternoon overpass for large urban areas in the US using GOME-2 and OMI observations.

90 To analyze the diurnal ~~variability~~ variation of NO_x in more detail, ~~instruments on geostationary satellites remote sensing instruments on satellites in geostationary orbit~~ are essential (Burrows et al., 2004). The South Korean instrument GEMS (Geostationary Environmental Monitoring Spectrometer, ~~(Kim et al., 2020)~~, Kim et al. (2020)) was launched in February 2020 and is the first instrument in geostationary orbit ~~that delivers from which~~ hourly daytime air quality ~~observations~~ data products, including NO₂, are retrieved. Positioned over the Equator at a longitude of 128.2°E, GEMS takes measurements with a spatial

95 resolution of about 3.5 km × 8 km over a large part of Asia. With up to 10 observations per day, GEMS ~~can offer valuable insights into the diurnal variability~~ data products offer a unique opportunity to investigate the diurnal variation of NO₂ and other trace gases. NASA's TEMPO (Zoogman et al., 2017) launched in April 2023 and ESA's Sentinel-4 (Ingmann et al., 2012) planned for launch in 2024 will provide similar observations over North America and Europe, respectively.

A study by Kim et al. (2023) evaluated GEMS L2 v1.0 total NO₂ ~~column data~~ VCD from November 2020 to January 2021

100 with four ground-based Pandora instruments, all located in Seosan, South Korea. They found correlation coefficients of 0.62–0.78 and an underestimation of the ground-based NO₂ measurements by the GEMS data set. Even though these four sites are relatively close together, they show different diurnal variations of NO₂, indicating that local transport or emissions have a significant influence. Zhang et al. (2023) evaluated their scientific POMINO-GEMS tropospheric NO₂ vertical column density (VCD) product with nine ground-based MAX-DOAS sites based on data from June–August 2021. The POMINO-GEMS

105 product shows a modest correlation of 0.66 with the MAX-DOAS observations and a reasonable agreement ~~of the observed diurnal variations~~ between the diurnal variations of the two data products but cannot achieve the much better correlation of 0.83 of the POMINO-TROPOMI product and the MAX-DOAS observations. Oak et al. (2024) showed that the main reason for differences between the operational GEMS L2 v2.0 and the operational TROPOMI NO₂ product is an incorrect use of the vertical coordinates in the NO₂ profiles for the GEMS AMF computation. GEMS and TROPOMI products, both based

110 on the same NO₂ vertical profile shapes, are in close agreement. Drivers of the diurnal variation of NO₂ observed by GEMS during winter and summer over Beijing and Seoul have been investigated by ~~Yang et al. (2023b)~~. They Yang et al. (2024). They used their own AMF and based their analysis on total NO₂ VCDs. With this, they found good agreement between the diurnal variations of total NO₂ ~~columns~~ VCDs in Pandora, GEMS, and GEOS-Chem ~~and~~. They used GEOS-Chem to interpret the observed variations ~~–Due and found that due~~ to high emissions at the two urban sites, NO₂ accumulates over the day, which is

115 offset by losses from chemistry and transport depending on season and wind speed. Edwards et al. (2024) used the GEMS L2 v2.0 tropospheric NO₂ VCD retrieval in combination with a chemical transport model to examine the NO₂ diurnal variation. Similar to Yang et al. (2024), they indicate different drivers for the diurnal variation on regional and local scales. Additionally, the model simulations show a high sensitivity to the assumed diurnal emission profile, especially on the local scale. A detailed

analysis of the impacts from diverse chemical transport model simulations and different underlying NO_x emissions on the GEMS NO₂ product has been conducted by Seo et al. (2024).

In this study, one year of tropospheric NO₂ VCDs ~~of retrieved by~~ the operational GEMS L2 v2.0 product, the scientific GEMS IUP-UB v1.0 product, the operational TROPOMI product, and 11 ground-based DOAS instruments in South Korea are compared. Evaluating the GEMS tropospheric NO₂ product-VCD is important to ~~ensure the accuracy of the product assess and quantify its accuracy~~ for use in ~~emission and surface concentration estimates~~ surface concentration and emissions applications (e.g., Xu et al., 2023; Yang et al., 2023b). The 11 ground-based observation sites are located in different pollution regimes in South Korea, which provides the opportunity to observe and analyze different diurnal variations of NO₂. Including the TROPOMI product in the comparisons adds an already well-validated reference data set around noon. ECMWF reanalysis v5 (ERA5) wind data at 10 m altitude give valuable insights into the influence of transport effects on the diurnal variation. Using a full year of data allows to analyze the influence of seasonality and the weekday-weekend effect on the GEMS tropospheric NO₂ VCD. The scientific GEMS IUP-UB NO₂ retrieval gives the possibility to change a priori assumptions such as the surface reflectivity and investigate its influence. Also the influence of different stratospheric corrections on the tropospheric NO₂ products is investigated.

The instruments and data sets included in this study are described in Sect. 2. After a first comparison of one month of averaged GEMS L2 v2.0, GEMS IUP-UB v1.0, and TROPOMI v02.04.00 tropospheric NO₂ VCDs maps in Sect. 3, one year of satellite ~~observations~~ tropospheric NO₂ VCDs is evaluated by comparisons with the tropospheric NO₂ VCD data set of the ground-based network distributed within South Korea (see Sect. 4.2) and car DOAS observations (see Sect. 4.3). In Sect. 5 the diurnal variations of the GEMS IUP-UB NO₂ ~~product-VCDs~~ and the ground-based observations are analyzed. ~~Influencing factors~~ Factors such as seasonality, wind speed, transport processes, and the weekday-weekend effect ~~are evaluated to understand the observed diurnal variation~~ that influence the tropospheric NO₂ VCD are investigated to better understand the origin of the observed diurnal variations. Possible reasons for deviations between GEMS and ground-based observations ~~are discussed.~~ such as the stratospheric correction, the surface reflectivity, and viewing geometry, are discussed in Sect. 5.4. A summary and conclusions are provided in Sect. 6.

2 Instruments and data sets

In this study, data from two measurement campaigns in South Korea are used: The GEMS Map of Air Pollution (GMAP) 2021 and the Satellite Integrated Joint Monitoring of Air Quality (SIJAQ) 2022 campaigns (<https://www.sijaq.org>). The main campaign periods ~~were took place~~ from October 2021 to November 2021 and May 2022 to August 2022. Some instruments were also operated between the main campaign periods and beyond. Analyses of this study focus on measurements taken between October 2021 and October 2022. One key aspect of these campaigns was to gather measurements for the validation and improvement of GEMS data, to better understand uncertainties and error sources in the satellite products, to support further improvement of the satellite retrieval algorithms, and to apply GEMS data for the characterization of air pollution.

Instruments from several teams participated in the campaigns. Measurements were delivered by stationary MAX-DOAS and

Pandora instruments, as well as mobile car DOAS instruments. ~~Details on~~ More details about the different instruments are provided below in Sect. 2.3 and 2.4. During the GMAP 2021 campaign, measurements were focused on the Seoul Metropolitan Area (SMA), ~~with having~~ a population of 26 million, one of the largest and most polluted metropolitan regions worldwide.

155 During the SIJQA 2022 campaign, measurements were additionally performed in the southern part of South Korea. This region includes Busan, the second largest city ~~of in~~ South Korea, and Ulsan, an important industrial center. Figure 1 shows GEMS observations of tropospheric NO₂ ~~vertical columns~~ VCDs over South Korea, indicating several pollution hot spots and the locations of the stationary instruments. The combination of stationary and mobile measurements makes a comprehensive validation of GEMS data possible. The stationary MAX-DOAS measurements are located in different pollution regimes and

160 provide daily measurements with ~~good a high~~ temporal resolution, but are restricted in spatial coverage to the area around the site, where each instrument is located. The car DOAS measurements lack temporal resolution but ~~can cover larger areas of a satellite pixel and can be operated over several satellite~~ are operated such that they make measurements within several satellite ground pixels in different regions to cover a large. This enables a variety of pollution levels and thus air quality conditions to be investigated. Table 1 lists all instruments involved in this study.

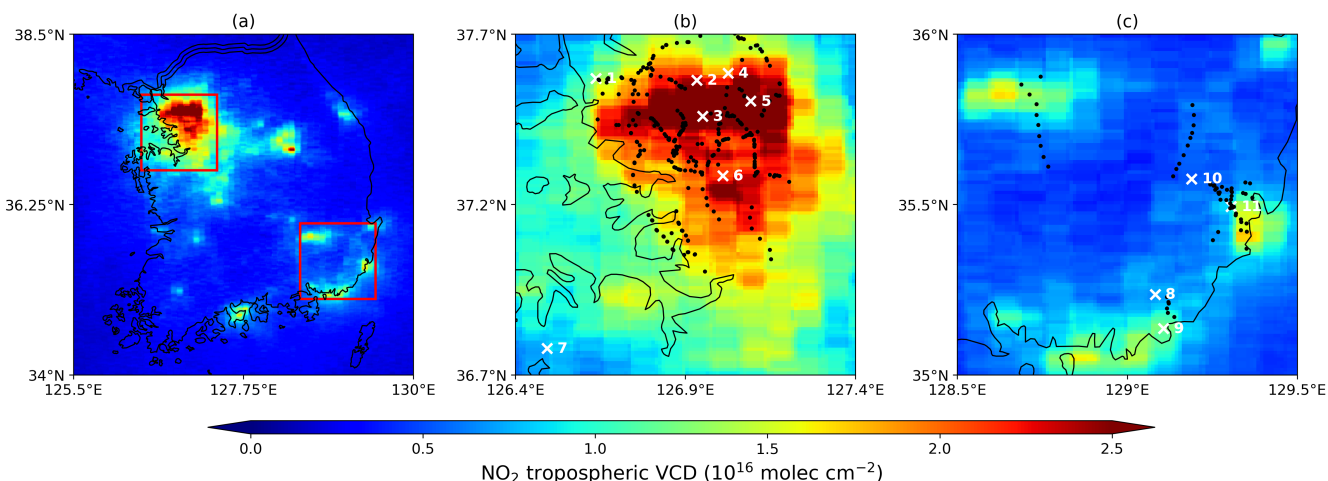


Figure 1. Maps of monthly mean NO₂ tropospheric ~~vertical columns~~ VCDs for South Korea ~~from~~. Panel (a) shows GEMS IUP-UB v1.0 observations in October 2021 around 13:45 Korean Standard Time (KST) (04:45 UTC). Panel (b) is a zoom into the SMA region indicated by the upper red rectangle in panel (a). Panel (c) is a zoom into the southeast, indicated by the lower red rectangle in panel (a). The white crosses show the locations of the ground-based measurement sites. The different instruments are listed together with the number given in Table 1. Black dots indicate locations of car DOAS observations used for GEMS validation.

165 2.1 Geostationary Environmental Monitoring Spectrometer (GEMS)

GEMS is a step-and-stare UV-visible imaging spectrometer onboard the satellite GK2B (Geostationary Korea Multi-Purpose Satellite 2), launched into geostationary orbit on 18 February 2020. It is the first geostationary mission to monitor air quality

Table 1. List of instruments included in this study with location, observation geometry, VCD retrieval information, and period of observation. MAX-DOAS BIRA Seoul (4) and MAX-DOAS BIRA Suwon (6) sites are using the same instrument, which was moved from Suwon to Seoul in December 2021.

Instrument	Location/Platform	Observation geometry	VCD retrieval	Available data
GEMS	GEO-KOMPSAT-2B	Step-and-stare, nadir	L2 v2.0 and IUP-UB v1.0	6-10 times/day
TROPOMI	Sentinel-5P	Push-broom, nadir	RPRO/OFFL v2.4.0	1-2 times/day (-13:30 KST)
MAX-DOAS IUP-UB Incheon (1)	Incheon (37.57° N, 126.64° E)	Multi-axis	FRM4DOAS 01.01 MMF	Oct 2021 - Oct 2022
Pandora 54 Yonsei (2)	Seoul (37.56° N, 126.93° E)	Multi-axis	PGN rnvh3.1-8	Oct 2021 - Oct 2022
Pandora 149 SNU (3)	Seoul (37.46° N, 126.95° E)	Multi-axis	PGN rnvh1 rnvh3.1-7-8	Oct 2021 - Oct 2022
MAX-DOAS BIRA Seoul (4)	Seoul (37.59° N, 127.03° E)	Multi-axis	FRM4DOAS 01.01 MMF	Dec 2021 - May 2022
MAX-DOAS MPIC Seoul (5)	Seoul (37.50° N, 127.09° E)	Multi-axis	FRM4DOAS 01.01 MMF	Oct 2021 - Aug 2022
MAX-DOAS BIRA Suwon (6)	Suwon (37.28° N, 127.01° E)	Multi-axis	FRM4DOAS 01.01 MMF	Oct 2021 - Dec 2021
Pandora 164 Seosan (7)	Seosan (36.78° N, 126.49° E)	Multi-axis	PGN rnvh3.1-8	Oct 2021 - Oct 2022
Pandora 20 Busan (8)	Busan (35.24° N, 129.08° E)	Multi-axis	PGN rnvh3.1-8	Oct 2021 - Oct 2022
MAX-DOAS MPIC Busan (9)	Busan (35.14° N, 129.11° E)	Multi-axis	FRM4DOAS 01.01 MMF	Jun 2022 - Aug 2022
Pandora 150 Ulsan (10)	Ulsan (35.24 35.57 ° N, 129.19° E)	Multi-axis	PGN rnvh3.1-8	Oct 2021 - Oct 2022
MAX-DOAS IUP-UB Ulsan (11)	Ulsan (35.49° N, 129.31° E)	Multi-axis	FRM4DOAS 01.01 MMF	Jun 2022 - Oct 2022
IUP car DOAS	Mobile car	Zenith-sky		campaign based
MPIC car DOAS	Mobile car	Zenith and 22°		campaign based
BIRA car DOAS	Mobile car	Zenith-sky		campaign based

hourly during the daytime. With its location at a longitude of 128.2°E over the Equator, GEMS covers a large part of Asia (5°S-45°S and 75°E-145°E). The ground pixels have a nominal resolution of approximately 3.5 km × 8 km over Seoul. GEMS is operated in 4 scan modes and allows up to 10 observations per day over the eastern part of the covered area, [including which includes](#) South Korea. Due to shorter days, the number of possible observations is reduced to 8 in March and October and is further limited to a maximum of six observations in winter. The GEMS spectrometer covers the wavelength range of 300-500 nm [with and has](#) a spectral resolution of 0.6 nm. The measurements yield ~~in~~-column amounts of O₃, NO₂, SO₂, HCHO, CHOCHO, and also aerosol and cloud information (Kim et al., 2020). We use the tropospheric NO₂ VCD of the operational [GEMS L2 v2.0](#) product and the scientific GEMS IUP-UB [v1.0](#) product, which are described below.

2.1.1 Operational GEMS L2 tropospheric NO₂ [VCD](#) product v2.0

The operational GEMS L2 tropospheric NO₂ [VCD](#) product v2.0 was reprocessed for the entire mission and is distributed by the National Institute of Environmental Research, NIER (<https://nesc.nier.go.kr/en/html/cntnts/91/static/page.do>). Data are available from 2021 onward. [GEMS irradiance data are wavelength calibrated using the pre-launch spectral response function.](#) [A single wavelength calibration is applied across all rows.](#) NO₂ slant column densities (SCDs) are retrieved ~~based on from~~ [Level 1 spectra using](#) a DOAS fit in ~~a the~~ fitting window of 432-450 nm. Using a lookup table of altitude-dependent air mass factors (AMFs) and ~~model-based model-based~~ vertical profile shapes, the NO₂ SCDs are converted into NO₂ VCDs. In v2.0,

the WRF-Chem + CAM-Chem model used in v1.0 (Lee et al., 2020), was replaced with the GEOS-Chem model, which has a spatial resolution of $0.25^\circ \times 0.3125^\circ$. The altitude-dependent AMFs from the radiative transfer model VLIDORT (Spurr, 2006) are tabulated as a function of the solar zenith angle (SZA), the viewing zenith angle (VZA), the relative azimuth angle (RAA), surface albedo, terrain height, temperature and pressure profiles, and aerosol parameters. The aerosol optical thickness (AOD), the single scattering albedo (SSA), and the aerosol layer height (ALH) are taken from GEMS L2 data. Since v2.0, the surface albedo is based on GEMS L2 surface reflectance data instead of the OMI climatology. The cloud correction of the AMF uses a linear combination of a clear-sky and a cloudy AMF, weighted by the cloud radiance fraction. The separation of the total NO₂ VCD ~~in~~ into its stratospheric and tropospheric parts is based on Bucselá et al. (2013), using GEOS-Chem model data for the tropospheric NO₂ column a priori and to mask high pollution regions.

To remove problematic retrievals and cloudy scenes, we use only ~~observations~~ GEMS data with a final algorithm flag of ~~1~~ 0 and a cloud fraction < 0.3 . The product provides the 'root_mean_square_error' resulting from the NO₂ fit but does not include errors from other retrieval aspects. Therefore, we ~~are estimating~~ estimate the tropospheric NO₂ VCD error based on the assessment done for the TROPOMI product with a typical value over continental polluted areas of $\pm 25\%$, which is dominated by the uncertainties in the AMF calculation (van Geffen et al., 2022).

2.1.2 Scientific GEMS IUP-UB tropospheric NO₂ VCD product v1.0

As part of the preparation for the European geostationary instrument on the satellite ~~S4~~ Sentinel-4, a scientific GEMS NO₂ product has been developed at the Institute of Environmental Physics at ~~University~~ the University of Bremen (IUP-UB). The GEMS L1 spectra are analyzed ~~with~~ using the DOAS technique in a larger fitting window from 405–485 nm and ~~with corrections in comparison to the operational GEMS L2 product, data are corrected~~ for instrument polarization sensitivity and scene inhomogeneity, and are de-striped. This results in less noise, a reduction of scatter, and improves the consistency with other products (TROPOMI, GOME-2) using similar large fitting windows. The retrieved SCDs are corrected for the stratospheric contribution based on the STRatospheric Estimation Algorithm from Mainz (STREAM, ~~(Beirle et al., 2016)~~ Beirle et al. (2016)). Tropospheric SCDs are converted into tropospheric VCDs with NO₂ a priori profile shapes from the TM5 chemical transport model (Williams et al., 2017) and a lookup table of altitude-dependent AMFs computed with the radiative transfer model SCIATRAN (Rozanov et al., 2014). The TM5 model has a spatial resolution of $1^\circ \times 1^\circ$. The altitude-dependent AMFs are tabulated as a function of SZA, VZA, RAA, surface albedo, and surface height. The surface albedo is based on the TROPOMI Lambertian equivalent reflectivity (LER) climatology (Tilstra et al., 2023). To evaluate the influence of the surface albedo, an additional version was created using the GEMS L2 surface reflectance data. The AMF cloud correction is based on the independent pixel approximation and uses recalculated cloud fractions and the cloud pressure from the GEMS L2 cloud product. The cloud fractions were computed from recalculated GEMS top of atmosphere (TOA) reflectances based on GEMS radiances and recalibrated irradiances by comparison with TOA reflectances modelled by SCIATRAN. In the current version of the algorithm, no aerosol correction is included. More details about the scientific GEMS IUP-UB tropospheric NO₂ v1.0 retrieval can be found in Richter et al. (in preparation, 2024).

Problematic retrievals and cloudy scenes with cloud radiance fractions of more than 50 % are removed ~~by~~ using only observa-

tions with a [quality assurance value \(qa_value\)](#) above 0.75. The ~~product quality flagging system is similar to that used in the operational TROPOMI product. However, the GEMS IUP-UB product does not yet have full error propagation and~~ contains the 'nitrogen dioxide tropospheric vertical column density uncertainty random', which, as in the operational product, only
220 contains the random error from the fit. The tropospheric NO₂ VCD error is estimated based on the same $\pm 25\%$ ~~assumption~~.

2.2 TROPOMI Tropospheric Monitoring Instrument (TROPOMI)

TROPOMI is a hyperspectral imaging spectrometer onboard the sun-synchronous near polar-orbiting satellite Sentinel-5P (S5P), launched in October 2017 (Veefkind et al., 2012). With its measurements in the UV, visible, and IR spectral regions, TROPOMI can monitor several atmospheric trace gases as well as clouds and aerosols. We use the tropospheric NO₂ [VCD](#)
225 product retrieved from measurements in the visible channel (400-496 nm). The ground pixel sizes are approximately 3.5 km \times 5.5 km in the middle of the swath. With orbit times of around 100 min and a wide swath of approximately 2600 km, TROPOMI has nearly global coverage and usually one to two overpasses per day in the mid-latitudes. Over the campaign region, TROPOMI provides observations between 12:28 and 14:40 Korean Standard Time (KST).

2.2.1 TROPOMI tropospheric NO₂ [VCD](#) product v02.04.00

230 The latest TROPOMI tropospheric NO₂ product, reprocessed for the entire mission, ~~is based on~~ [uses](#) processor version 02.04.00. The v02.04.00 product was generated operationally from 17 June 2022 to 12 March 2023. We are using the offline (OFFL) as well as the reprocessed (RPRO) data of this version, which is available from the Sentinel-5P Pre-Operations Data Hub (last access: 21 February 2022). The following processor versions had only minor bug fixes and have not yet been
235 applied to the full data set (Eskes and Eichmann, 2023). The Level 1b version 2.1 spectra are analyzed with the DOAS technique in a fitting window of 405-465 nm to retrieve NO₂ SCDs. The retrieved SCDs are separated into their stratospheric and tropospheric parts with NO₂ vertical profile information from the 1° \times 1° TM5 global chemistry transport model and a data assimilation system that assimilates TROPOMI SCDs. Using a lookup table of altitude-dependent AMFs and actual daily TM5 NO₂ vertical profile shapes, the resulting tropospheric SCDs are converted into tropospheric VCDs. The altitude-dependent AMFs are a function of SZA, VZA, RAA, surface albedo, surface pressure, and (mid-level) atmospheric pressure.
240 Since v02.04.00, the surface albedo in the NO₂ spectral fitting window and in the cloud pressure retrieval is based on the TROPOMI directionally dependent LER (DLER) climatology (Tilstra et al., 2023). The cloud radiance fraction is retrieved from the NO₂ spectral region at 440 nm. The cloud pressure retrieval is based on the FRESCO-wide algorithm in the NIR spectral range. In the AMF, ~~clouds and indirectly~~ [both clouds and, indirectly](#), aerosol loads are accounted for [by](#) using a linear combination of a clear-sky and a cloudy AMF, weighted by the cloud radiance fraction (van Geffen et al., 2022).
245 To remove problematic retrievals, we are using only observations with the recommended qa_value above 0.75. This also removes scenes with cloud radiance fractions in the NO₂ window of more than 50% (Eskes and Eichmann, 2023). The TROPOMI NO₂ product contains the data field 'nitrogen dioxide tropospheric column precision', which provides the error estimate originating from the NO₂ fit and other retrieval aspects that ~~is~~ [are](#) dominated by the uncertainty in the tropospheric ~~air-mass factor (\pm AMF of 25 %)~~.

250 2.3 MAX-DOAS observations and data sets

The satellite tropospheric NO₂ VCDs are compared to collocated MAX-DOAS ~~observations~~tropospheric NO₂ VCDs. We use data from MAX-DOAS instruments at six sites in South Korea, ~~from which four~~. Four sites were located in the northern campaign region and two in the southeastern campaign region (see Table 1). Not all of them have been operated over the whole year. ~~Data availability for satellite validation is also visible in~~of measurements. The data availability for the satellite
255 validation can be seen in the Appendix Fig. A8. The ground-based MAX-DOAS instruments measure the UV-visible scattered sunlight in several azimuthal directions and elevations. The ~~here used~~tropospheric NO₂ VCDs are used in this study were retrieved by applying the Mexican MAX-DOAS Fit (MMF; ~~(Friedrich et al., 2019)~~Friedrich et al. (2019)) inversion algorithm using the FRM4DOAS (v01.01, <https://frm4doas.aeronomie.be/>) settings and setup (Hendrick et al., 2016). The product is quality filtered using only data with a recommended 'qa_flag_no2' of 0 and 1. This quality flag uses additionally the Mainz
260 profile algorithm (MAPA, ~~(Beirle et al., 2019b)~~; Beirle et al. (2019b)) data in the quality check. Details about the implemented algorithms and quality flagging approaches can be found in Hendrick et al. (in preparation, 2024). To ensure comparability between the MAX-DOAS instruments from different institutes, ~~there was an inter-comparison period~~an intercomparison period was conducted at the beginning of the campaign, ~~during which all instruments except~~. During this period, all instruments, except for the MAX-DOAS IUP-UB Ulsan, were operated at the same location. The comparisons show very good correlations
265 between the instruments. The inter-comparison results are presented in Hendrick et al. (in preparation, 2024). The Pandonia Global Network (PGN, <https://www.pandonia-global-network.org>) is a network of ground-based UV-visible spectrometers called Pandora, which focuses on total column observations from direct sun measurements, but ~~can also provide~~also provides tropospheric column observations when operated in multi-axis mode. We use data from the five Pandora instruments, located in South Korea that are operated in the multi-axis mode. Three of them are located in the northern campaign
270 region, and two are in the southeastern region. Data are processed as part of the PGN Pandonia Global Network (last access: 4 February 2023). All data ~~except for the Pandora SNU~~ are on the processor version 1.8 and retrieval version nvh3. ~~Data of the Pandora SNU are only available in processor version 1.7 with retrieval version nvh1. The most important update between the versions is a more stringent quality filtering. We only use data with quality flags indicating high and medium quality and filter data of low quality or~~ We filter data which are flagged as unusable (~~flags 2, 12, 20, 21, and 22~~) and additionally for wrms
275 (normalized rms of fitting residuals weighted with independent uncertainty) larger than 0.002. Details on the retrieval of the tropospheric NO₂ VCD and the respective uncertainty can be found in Cede (2021).

2.4 Car DOAS instruments and data sets

During the GMAP 2021 and SIJAQ 2022 main campaign periods, mobile car DOAS measurements were performed by instruments of the IUP-UB, the Max Planck Institute for Chemistry in Mainz (MPIC), and the Royal Belgian Institute for Space
280 Aeronomy (BIRA). To achieve high spatial resolution over the covered area, the majority of measurements was taken in zenith-sky with some off-zenith measurements. Instruments were operated in both campaign regions and synchronized to the GEMS schedule to cover several GEMS observations throughout the day. Compared to the stationary data, the car measurements have

the advantage that they can cover larger and more diverse areas. The car DOAS data analysis was done independently by the operating institutes. More details about the car DOAS instruments and the tropospheric NO₂ VCD retrieval can be found in Lange et al. (2023).

3 Satellite tropospheric NO₂ products product comparison

Before comparing the satellite tropospheric NO₂ VCD products with ground-based measurements, an assessment of the three products based on maps of monthly averaged observations provides first insights into tropospheric NO₂ VCDs provides a first assessment of the differences between the two GEMS NO₂ products and the TROPOMI product. Figure 2 shows maps of the tropospheric NO₂ VCDs for South Korea from GEMS L2 v2.0 (a), GEMS IUP-UB v1.0 (b), and TROPOMI v02.04.00 (c) observations in October 2021. For better comparison, the two GEMS data sets are averaged only for the 13:45 KST (04:45 UTC) observation, which is close to the TROPOMI overpass between 12:28 KST and 14:37 KST. Data are sampled at 0.01° resolution. As the AMF of the GEMS L2 v2.0 NO₂ product is not interpolated in space, the map of the tropospheric NO₂ VCDs (a) shows box structures with boxes of the same size as the spatial resolution of the GEOS-Chem model.

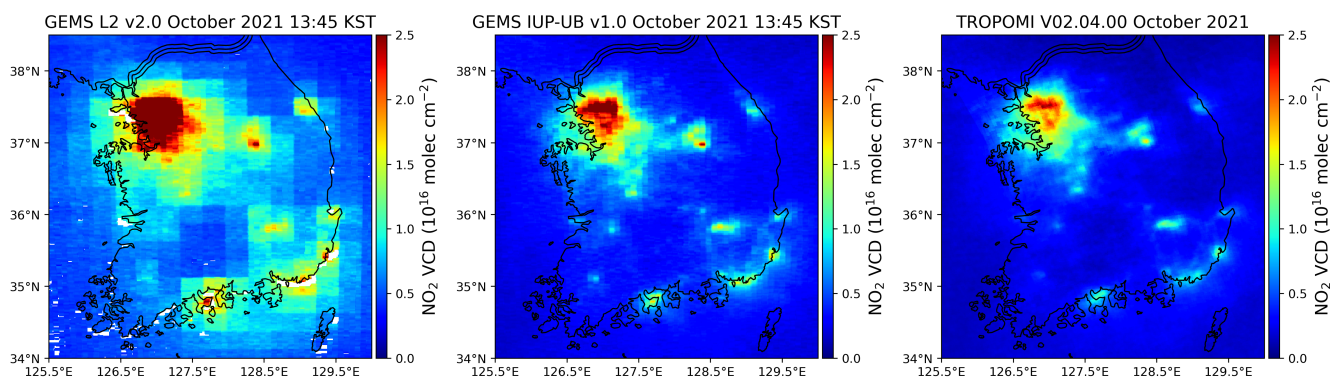


Figure 2. Maps of NO₂ tropospheric VCD for South Korea from GEMS L2 v2.0 (a), GEMS IUP-UB v1.0 (b), and TROPOMI v02.04.00 (c) observations in October 2021. The GEMS data sets are averaged for the 13:45 KST (04:45 UTC) observation close to the TROPOMI overpass. All data sets are cloud and quality filtered.

All three maps show the dominant hot-spot of elevated NO₂ concentrations centered over the SMA and several smaller hot-spots elevated NO₂ regions with the Danyang county, including Jecheon and a mining area in the mid-north, Donghae on the east coast, Gwangyang in the south, and Daegu, Pohang, Ulsan, and Busan in the southeast. These hot-spots regions of elevated NO₂ show the highest values in the GEMS L2 tropospheric NO₂ VCD product, especially over the SMA, followed by the GEMS IUP-Bremen product and the lowest values in the TROPOMI product. Additionally, we note that the background NO₂ is similar in the TROPOMI and GEMS IUP-UB products but significantly higher in the GEMS L2 product. This difference in the background NO₂ can be caused by the different stratospheric corrections used in the three products (GEOS-Chem with

GEMS data assimilation, STREAM, and TM5 with TROPOMI data assimilation). These are discussed further in Sect. 5.4. The influence of the stratospheric correction will be visible most prominently in the evaluation with the ground-based data for stations located in remote low-polluted regions such as the Pandora Ulsan (8, see Fig. 1). As the AMF is not interpolated in space, the map of the GEMS L2 v2.0 NO₂ product shows box structures with boxes of the same size as the spatial resolution of the GEOS-Chem model. which is located at the Ulsan National Institute of Science and Technology, several kilometers outside the city and industrial area of Ulsan, or the Pandora Seosan (instruments 10 and 7, see Fig. 1). The map of the TROPOMI NO₂ product appears the most smoothed, caused by the orbital cycle of 16 days and the resulting oversampling. Since GEMS maintains a constant ground pixel pattern for each of the four scan modes, there is no oversampling and smoothing, which makes the sampling pattern visible in the GEMS averages. Missing data in the GEMS L2 v2.0 NO₂ product, which are mainly visible in coastal regions, are caused by the product's quality filter.

4 Evaluating satellite tropospheric NO₂ VCD with ground-based data

~~The large data set of the~~

4.1 Collocation criteria - method

~~Stationary ground-based instruments distributed in South Korea is used to evaluate the satellite tropospheric NO₂ VCD product.~~ ~~Ground-based data VCDs~~ are averaged within ± 20 min of the satellite ~~observation overpass~~ and compared to the closest satellite pixels extracted within a radius of 5 km around the station sites. Other criteria for co-location were tested, e.g., including larger areas, area averaging, and considering the ground-based instruments VAA during the satellite overpass. Some of the results are shown in Fig. A3 in the Appendix. The results are either slightly worse or not significantly better than the nearest pixel approach. This is in contrast to Dimitropoulou et al. (2020), who showed significant improvements in slope and correlation when considering the directional dependency for a comparison of TROPOMI and MAX-DOAS observations in Uccle, Belgium. Therefore, further investigations are required into why the comparisons in South Korea behave differently. All linear regression statistics in this study are calculated with orthogonal distance regression (ODR) to take into account the error in both evaluated and reference measurements. The correlation between the evaluated and reference measurements is described by the Pearson correlation coefficient (r). Additionally, the median relative difference (mrd) is calculated by the following convention:

$$\text{median relative difference}(\%) = \frac{(\text{evaluated} - \text{reference})}{\text{reference}} \cdot 100 \quad (1)$$

The evaluated measurements are the satellite tropospheric NO₂ VCDs. The reference measurements are either the stationary ground-based or the mobile car DOAS tropospheric NO₂ VCDs in Sect. 4.3.

4.2 Evaluating satellite tropospheric NO₂ VCD with MAX-DOAS and Pandora

The large data set of ground-based instruments distributed in South Korea is used to evaluate the satellite tropospheric NO₂ VCD product. Scatter plots of all coincident satellite and stationary ground-based measurements are shown in Fig. 3 for the GEMS L2 (panel a), the GEMS IUP-UB (panel b), and the TROPOMI (panel c) NO₂ tropospheric VCD products. Since all 6-10 observations per day are considered for the comparisons of the GEMS products to the ground-based data set, there are 7928-8405 coincident measurements for the GEMS L2 and 11823-12999 for the GEMS IUP-UB product, which is many more than for the TROPOMI product with 1624-1707. A comparison limited to the TROPOMI overpass time between 12:28 KST and 14:37 KST is shown in the Appendix Fig. A1. Same as Fig. 3 but GEMS L2 and GEMS IUP-UB observations are limited

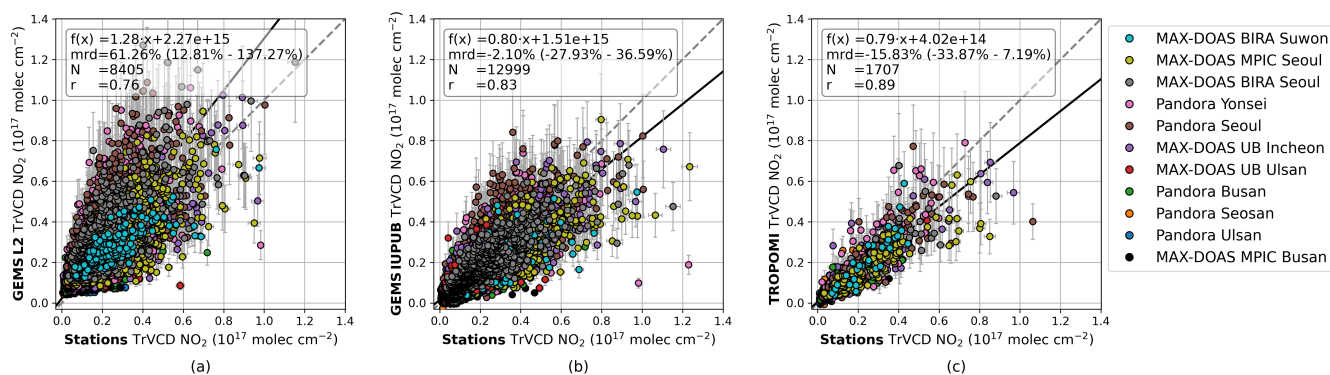


Figure 3. Scatter plots of GEMS L2 (a), GEMS IUP-UB (b), and TROPOMI (c) NO₂ tropospheric VCDs vs. co-located ground-based NO₂ tropospheric VCDs. The ground-based observations are considered co-located if they are taken within ± 20 min around the satellite observation. Measurements within this period are averaged and matched to the closest satellite observation within a radius of 5 km around the station site. The error bars represent the tropospheric NO₂ VCD error. Points are colored according to the corresponding ground-based instrument. The dashed gray line indicates the 1:1 line. The solid black line represents the orthogonal distance regression.

to the TROPOMI overpass time between 12:28 KST and 14:37 KST. The difference in the number of coincident measurements between the GEMS L2 and the GEMS IUP-UB product is mainly caused by the stricter quality filter of the GEMS L2 product. Limiting the filter process of the GEMS L2 product on the cloud filter only, results in a more comparable number of data points. All linear regression statistics in this study are calculated with orthogonal distance regression (ODR) to take into account the error in both evaluated and reference measurements. The correlation between the evaluated and reference measurements is described by the Pearson correlation coefficient r . Additionally, the median relative difference is calculated by the following convention:-

$$\text{median relative difference}(\%) = \frac{(\text{evaluated} - \text{reference})}{\text{reference}} \cdot 100$$

The evaluated measurements are the satellite tropospheric NO₂ VCDs. The reference measurements are either the stationary ground-based or the mobile car DOAS tropospheric NO₂ VCDs. For satellite and ground-based matched, the coincidence criterion is described above. For the satellite and car DOAS coincidence criteria, see Sect. 4.3. The GEMS L2 and ground-based tropospheric NO₂ VCDs are correlated with have a Pearson correlation coefficient of $r = 0.750.76$, with a slope of

1.271.28, a median relative bias of +64.61 %, and an offset of $2.73 \times 10^{15} \text{ molec cm}^{-2}$ ~~2.27 $\times 10^{15} \text{ molec cm}^{-2}$~~ . This overestimation is in contrast to the underestimation visible in the GEMS IUP-UB and TROPOMI NO₂ products. Potential explanations for this different bias, such as the surface reflectivity used for the AMF determination, [the stratospheric correction](#) and the consideration of aerosol parameters, are further discussed in Sect. 5.4. ~~With a slope of 0.81 and a median bias of -1 % for the~~ [The GEMS IUP-UB and a slope of as well as the TROPOMI product show a slight underestimation, with slopes of 0.80, respectively 0.79, and a median bias of -14.2 % for the TROPOMI product, both products show a slight underestimation. This kind and -16 %.](#) A similar magnitude of underestimation of satellite [tropospheric NO₂ products compared VCDs relative](#) to ground-based observations has been observed in many validation studies for satellite data sets (e.g., Ma et al., 2013; Verhoelst et al., 2021) and is often explained by local NO₂ hot spots that are not resolved in the satellite data and the a priori fields used for the AMF calculations. Another reason ~~can be is~~ [the missing aerosol correction in these satellite products.](#) When binning the median relative differences of the GEMS IUP-UB and MAX-DOAS comparison by the AOD, determined in the FRM4DOAS MAX-DOAS analysis, an increasing bias is observed with an increase in the AOD (see Appendix Fig. A2). This was similarly observed for a comparison of tropospheric NO₂ VCDs of MAX-DOAS and TROPOMI (Lambert et al., 2023).

365 The GEMS IUP-UB product, considering all observations per day, has a good correlation with a coefficient of 0.82 but is more scattered than the TROPOMI product, which is limited to its noon observation time. To investigate whether the better correlation of the TROPOMI product is attributed to the data itself or the timing of the satellite overpass, all data sets were limited to the period corresponding to TROPOMI overpasses. ~~For, see Appendix Fig. A1. For both, the GEMS L2 product, this limitation amplifies the overestimation with a slope of 1.41 compared to 1.27 and a median bias of +64 % compared to +85 %~~ [but improves the correlation from 0.75 to 0.79. For the and the GEMS IUP-UB product, the time limit increases the slope and median bias increase from 0.81 to 0.89, respectively -1 % to +7 % and brings the correlation of the GEMS IUP-UB product to 0.85, close to the very good correlation of the TROPOMI NO₂ products slightly and reduces the scatter.](#) This indicates larger deviations between the GEMS and ~~MAX-DOAS observations~~ [ground-based tropospheric NO₂ VCDs](#) in the morning and/or afternoon, which will be further analyzed by comparing the diurnal [variability variation](#) in Sect. 5.

375 ~~The comparisons are based on coincident measurements considering the closest pixels within a radius of 5 km around the station sites. However, we have also compared the ground-based measurement with the closest pixels within a radius of 10 km, averaging all pixels within a radius of 5 km, respectively 10 km, and considering the viewing azimuth angle (VAA) of the ground-based instruments to account for spatial inhomogeneity. The results are shown in Fig. A3 in the Appendix. To investigate the VAA dependence, the GEMS pixels VCD_{sat} are weighted according to their contribution along the line of sight~~ [d of the ground-based instruments.](#)

$$\text{VCD}_{\text{sat, VAA}} = \frac{\sum \text{VCD}_{\text{sat } i} \cdot d_i}{\sum d_i}$$

~~We consider the line of sight within 5 km to the station site. The comparison is only included in the analysis when more than 75 % of the line of sight is covered by satellite pixels. Since ground-based measurements taken within ± 20 min of the satellite observation in different VAA are considered independently, this comparison results in more coincident data points.~~ [Measurements taken in the same VAA, overlapping with the same GEMS pixels, are averaged within the time window. Even](#)

if a better representation of spatial inhomogeneity is expected with this comparison, the results are either slightly worse or not significantly better than the nearest pixel approach. This is the same for all three satellite products. Also, additional averaging of the VAA comparisons within the ± 20 min time window does not improve the comparisons. This is in contrast to Dimitropoulou et al. (2020), who showed significant improvements in slope and correlation when considering the directional dependency for a comparison of TROPOMI and MAX-DOAS observations in Uccle, Belgium. Therefore, further investigations are required into why the comparisons in South Korea behave differently.

4.3 Comparison of satellite and ground-based tropospheric NO₂ VCDs for the individual sites

When separating the comparison of the satellite and ground-based observation into the individual sites, quite some differences can be observed between the different sites. Figure A5 shows the scatter plots of GEMS IUP-UB tropospheric NO₂ individual sites. Figure 4 shows box-and-whisker plots for the three satellite NO₂ VCDs vs. co-located ground-based NO₂ tropospheric VCDs for the 11 stations. The correlation varies between 0.67 for the MAX-DOAS IUP-UB Ulsan site and 0.87 for the MAX-DOAS IUP-UB Incheon site. The slope varies between 0.40 for the MAX-DOAS MPIC Busan site and 1.17 for the Pandora SNU at Seoul National University (SNU). Scatter plots for the GEMS L2 and TROPOMI products can be found in the Appendix Fig. A4 and A6. products and all stations summarizing the bias and spread of the differences. For the GEMS L2

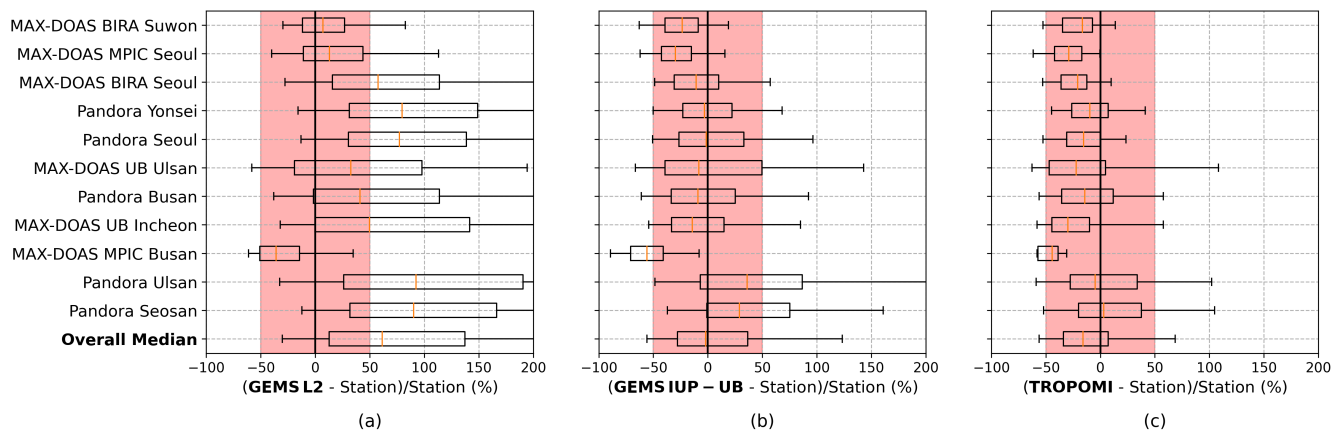


Figure 4. Box-and-whisker plots summarizing the bias and spread of the difference between the (a) GEMS L2, (b) GEMS IUP-UB, (c) the TROPOMI and the individual ground-based tropospheric NO₂ VCDs. Stations are ordered from bottom to top by increasing median ground-based tropospheric VCD. The orange line inside the box represents the median relative difference. Box bounds mark the 25 and 75 % quantiles. Whiskers represent the 5 and 95 % quantiles. The red-shaded area represents a bias of ± 50 %.

product, differences between the individual sites are even larger due to the dependence on the AMF box in which the station is located (see Fig. 2). Figure 4 shows box-and-whisker plots for the three satellite NO₂ VCDs vs. co-located ground-based NO₂ tropospheric VCDs. The large negative bias for the MAX-DOAS MPIC Busan site is visible in all product comparisons and is possibly caused by its location close to the coast (<500 m) and the associated inhomogeneities. The sea-land breeze circulation can create complex horizontal and vertical gradients in

atmospheric composition, which are difficult to resolve in a priori profiles used for satellite retrievals (e.g., Souri et al., 2023).
405 Furthermore, the measurements of this instrument are performed in an azimuth direction of 253°, which crosses the port of Busan, a local source of NO_x. In general, there is a slight tendency to larger biases for more polluted sites while less-polluted sites show differences closer to 0. These findings are similar to the validation results from Verhoelst et al. (2021) on TROPOMI NO₂ products and all stations summarizing the bias and spread of the differences. Scatter plots of GEMS IUP-UB tropospheric NO₂ VCDs vs. co-located ground-based NO₂ tropospheric VCDs for the 11 individual sites. Station names and measurement
410 periods can be found in the title. Co-location criteria are with ± 20 min and nearest 5 km the same as in Fig. 3. Plots showing the comparisons for the GEMS L2 and TROPOMI products can be found in the Appendix Fig. A4 and Fig. A6. Box-and-whisker plots summarizing the bias and spread of the difference between the (a) GEMS L2, (b) GEMS IUP-UB, (c) the TROPOMI and the individual ground-based tropospheric NO₂ VCDs. Stations are ordered from bottom to top by increasing median ground-based tropospheric VCD. The orange line inside the box represents the median relative difference. Box bounds mark the 25 and 75 % quantiles. Whiskers represent the 5 and 95 % quantiles. The red shaded area represents a bias of ± 50 %. Plots with observations limited to the TROPOMI overpass time can be found in the Appendix Fig. ?? data. The positive bias in the GEMS IUP-UB for the Pandora Ulsan and the Pandora Seosan, both less polluted sites, could indicate an underestimation of the stratospheric contribution at these sites.

The overall bias (median of all satellite and station pair differences) is +64.61 % (13 % - 137 % interquartile range) for the GEMS
420 L2 product, -1.2 % (-28 % - 37 %) for the GEMS IUP-UB product, and -14.16 % (-34 % - 7 %) for the TROPOMI product. A comparison by Lambert et al. (2023) based on tropospheric NO₂ VCDs of the Network for the Detection of Atmospheric Composition Change (NDACC) MAX-DOAS data from 29 stations and TROPOMI data of v2.4.0 and 2.5.v2.5.0 from May 2018 to November 2023 shows a median bias of -28 % and for a subset of 8-eight MAX-DOAS stations in the TROPOMI Validation Data Analysis Facility Automated Validation Server (VDAF-AVS) of -17.5 %. Thus somewhat larger than for the
425 data set analyzed here. For the GEMS IUP-UB and the TROPOMI product, the overall and the individual biases, except for the MAX-DOAS MPIC Busan, are within the typical mission requirement of a maximum bias of 50 % (van Geffen et al., 2022). The large negative bias for the MAX-DOAS MPIC Busan site is visible in all product comparisons and is possibly caused by its location close to the coast (<500) and the associated inhomogeneities. The sea-land breeze circulation can create complex horizontal and vertical gradients in atmospheric composition, which are difficult to resolve in a priori profiles used
430 for satellite retrievals (e.g., Souri et al., 2023). Furthermore, the measurements of this instrument are performed in an azimuth direction of 253°, which crosses the port of Busan, a local source of NO_x. There is a slight tendency to larger biases for more polluted sites while less polluted sites show differences closer to 0. These findings are similar to the validation results from Verhoelst et al. (2021) on TROPOMI NO₂ data. The positive bias in the GEMS IUP-UB for the Pandora Ulsan and the Pandora Seosan, both less polluted sites, could be an indication for an underestimation of the stratospheric contribution at these
435 sites. In general, it can be concluded that the GEMS IUP-UB product and the TROPOMI product show good agreement in the individual biases, supporting the good agreement visible in the overall comparison. The agreement which is improved when limiting the GEMS IUP-UB product comparisons to the TROPOMI overpass time. Scatter plots of the satellite products vs. the co-located ground-based data for the 11 individual stations can be found in the Appendix (Fig. A4, Fig. A5, Fig. A6).

4.3 Comparison of GEMS IUP-UB and car DOAS observations

440 The car DOAS ~~observations~~tropospheric NO₂ VCDs are used, in addition to the stationary ground-based observations, to evaluate the GEMS IUP-UB tropospheric NO₂ VCDs. The IUP, MPIC, and BIRA car DOAS instruments were operated in the two campaign regions. Considering that the car DOAS data used for this comparison were analyzed independently by the different groups and with only partly harmonized retrieval methods with different assumptions, the data show good agreement and provide an additional data set for the evaluation of GEMS data. The locations of the car DOAS observations are displayed

445 in Fig. 1. Compared to the stationary data, they can cover larger and more diverse areas, which is reflected in the large range of NO₂ values shown in Fig. 5. The scatter plot shows GEMS IUP-UB tropospheric NO₂ VCDs vs. co-located car DOAS NO₂ tropospheric VCDs. The car DOAS data are compared to the GEMS pixel in which they were measured, averaged ± 20 min around the GEMS observation. In total, 1146 pairs of coincident measurements are considered, of which 272 were taken during the TROPOMI overpass time window. The comparison between the GEMS IUP-UB and the car DOAS data shows a

450 good correlation with a correlation coefficient of 0.87. ~~Thus, they are better correlated than the stationary ground-based data with a correlation of 0.82.~~ The slope of 0.7 and a median relative bias of -30% ~~;~~ indicatesindicate a larger negative bias than the comparison with the stationary ground-based data set. This larger underestimation of the GEMS IUP-UB product may be caused by the bias of the larger proportion of high NO₂ ~~observations~~tropospheric VCDs, which was already visible from the

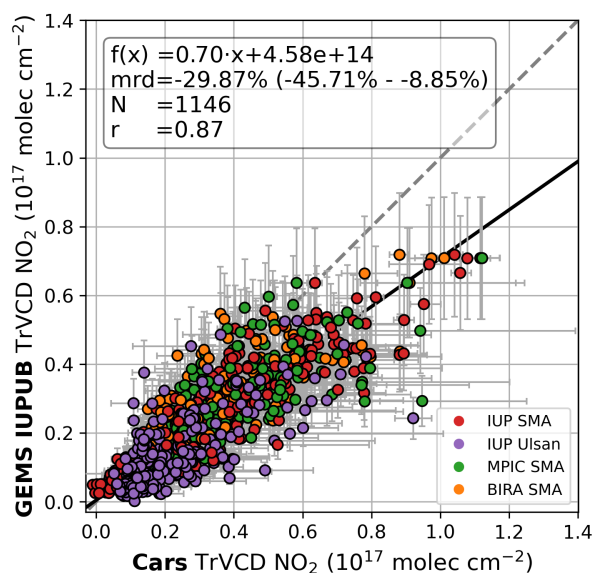


Figure 5. Scatter plot of GEMS IUP-UB tropospheric NO₂ VCDs vs. co-located car DOAS NO₂ tropospheric VCDs. The car DOAS observations are considered co-located if they are taken ± 20 min around the time of the GEMS observation-measurement within the satellite pixel. Each point is colored by the respective car DOAS instrument. Vertical ~~error~~error-bars represent the tropospheric NO₂ VCD error. Horizontal ~~error~~error-bars are the 10th and 90th percentile to illustrate the spatiotemporal variability.

evaluation by individual stations for the more polluted sites. ~~Considering that the car DOAS data used for this comparison were analyzed independently by the different groups and with only partly harmonized retrieval methods with different assumptions, the data show good agreement, providing an additional data set for the evaluation of GEMS data.~~ Horizontal error bars represent Horizontal bars indicate the 10th and 90th percentile of car DOAS observations within the GEMS pixel and ± 20 min time intervals to illustrate the spatiotemporal variability. These ~~error~~ bars can become relatively large, indicating the considerable temporal and spatial ~~natural variability of~~ variability of tropospheric NO_2 even within the GEMS pixel. Further investigations based on the car DOAS observations can provide more insights into the representativeness of observations and the natural variability of NO_2 .

5 Diurnal variation of GEMS and ground-based tropospheric NO_2 VCDs

~~As GEMS is the first geostationary instrument able to observe the diurnal variation of NO_2 , it is interesting to compare the diurnal variation found in the GEMS data with those.~~ We assess the agreement between the diurnal variation observed by GEMS and that observed by the ground-based instruments. ~~In Fig. ??, interpreting the observed diurnal variations and their differences is difficult as they are driven by emissions, the chemistry of NO_x , and transport processes. These factors vary with season, wind speed, transport processes, and weekday-weekend effects, and are analyzed in more detail in the following sections.~~

5.1 Seasonality

470 Figure 6 shows the observed diurnal variation divided into winter (DJF), spring (MAM), summer (JJA), and autumn (SON) from the median diurnal variation of the GEMS IUP-UB product and the ground-based station data are shown for 10 of the 11 stations. The diurnal variability of tropospheric NO_2 VCDs from the GEMS L2 v2.0 product and ground-based observations can be found in the Appendix Fig. ??, and the station's data sets for those stations which were operated over the whole year, six out of the eleven stations. ~~Due to limited data availability at the MAX-DOAS MPIC Busan site, it is not shown here.~~
475 ~~Also, the MAX-DOAS BIRA Suwon and the MAX-DOAS IUP-UB Ulsan sites have limited data due to their relatively short operation time, indicated in the green bar at the top of each plot. However, eight sites have a large enough data set, which can be compared to the diurnal variability seen in the GEMS data.~~ The ~~At the sites within the SMA (Incheon, Yonsei, Seoul), mean tropospheric NO_2 VCDs are larger than at the other sites, and the diurnal variation can be quite different between the individual sites (see also Chong et al. (2018)) and differ additionally between the seasons. However, the~~ overall behavior of the GEMS
480 IUP-UB and the ground-based data are very similar. ~~However, the two most polluted sites, the MAX-DOAS MPIC Seoul and the MAX-DOAS BIRA Suwon show a clear low bias of the GEMS IUP-UB data, already seen in Fig. 4. This underestimation is visible throughout the whole day but is largest in the morning.~~ The low-polluted sites, the Pandora Seosan and the Pandora Ulsan ~~show,~~ show little diurnal variation and a high bias of the GEMS IUP-UB ~~data~~ tropospheric NO_2 VCD, which is relatively stable over the day. For the Pandora Seoul site, the GEMS IUP-UB product overestimates the station columns in autumn,
485 but both show very similar diurnal variation. The other sites show ~~good agreement, especially the best agreement~~

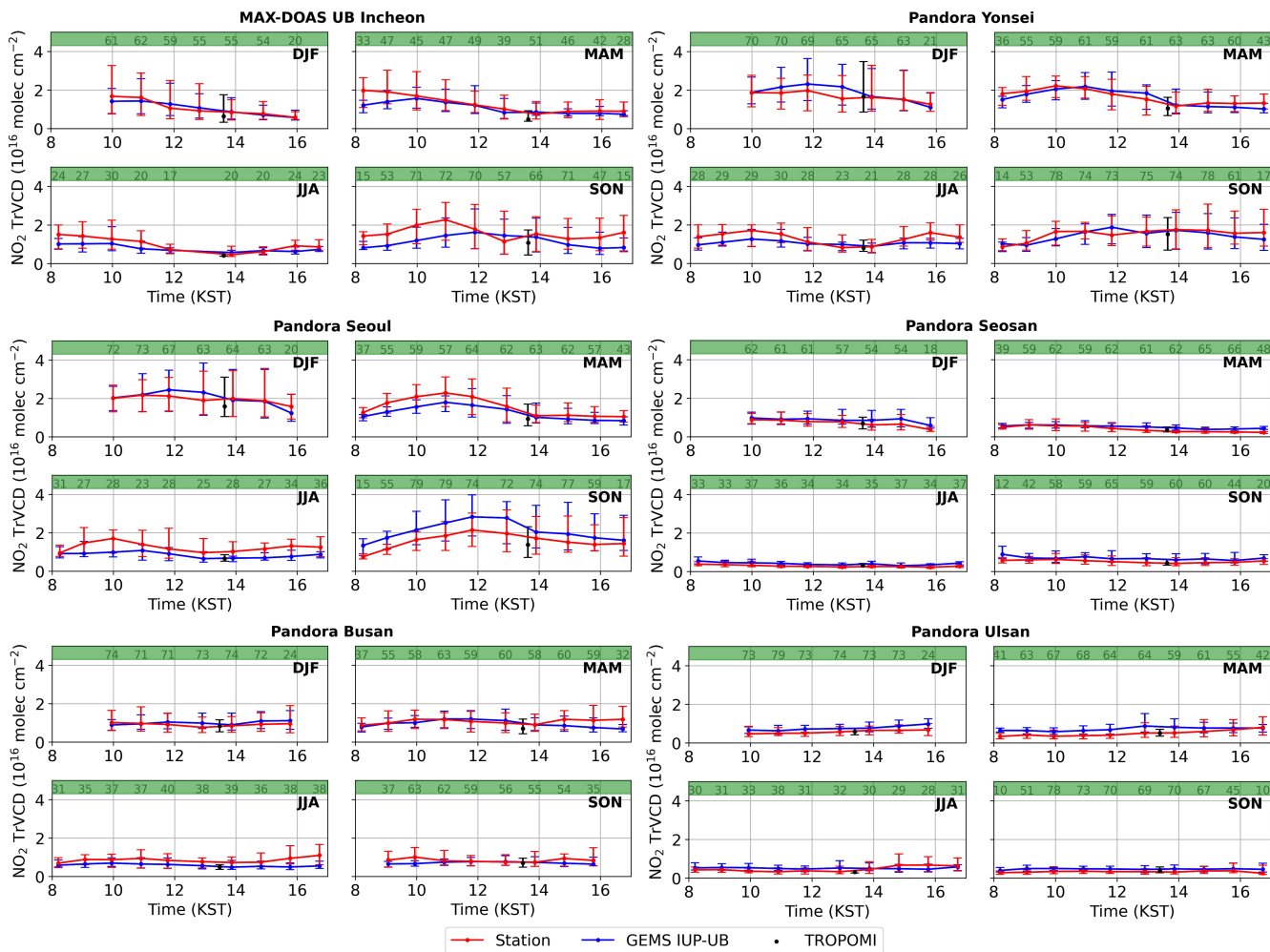


Figure 6. Diurnal variability-variation of the median tropospheric NO₂ VCDs from the GEMS IUP-UB product (blue) and ground-based stations (red) for the individual seasons (DJF, MAM, JJA, SON). The TROPOMI observation is added in black. Error-Station names can be found in the individual titles. Vertical bars represent the 25 and 75 % quantiles of the MAX-DOAS and GEMS observations. The numbers in the green bar represent the number of GEMS and MAX-DOAS observations that contributed to the median value observations. Station names and measurement periods-Plots for the GEMS L2 product can be found in the individual titles Appendix Fig. A7.

noon from around 11 to 14 KST. Deviations are visible Several stations show deviations in the morning and late afternoon, where the GEMS IUP-UB product often underestimates the station values, which is most for example visible prominently for the MAX-DOAS UB Incheon, in summer and autumn, and the Pandora Yonsei, and especially the MAX-DOAS BIRA Seoul site. These biases are summarized in Fig. A9, which shows the diurnal variability of the median relative differences of the in summer. For the Pandora Busan site, the underestimation of the GEMS IUP-UB NO₂ product at the individual sites. Diurnal variability of the median relative differences of the GEMS IUP-UB NO₂ product at the different ground-based sites.

Stations are color-coded. The median relative difference, including differences of all stations, is shown as black bars. Error bars represent the 25 and 75 % quantiles. Results are only included if more than 20 observations are available per time bin and station. This shows, as discussed, the best agreement around noon and the larger biases in the product is strongest in the late afternoon, especially during spring and summer. These deviations during the morning and late afternoon , especially for the 16:45 KST observation where the GEMS IUP-UB NO₂ product underestimates all sites observations except for the Pandora Seosan. It is interesting to see that the diurnal variation can be quite variable between the different sites. The Seoul stations (Pandora-SNU, MAX-DOAS MPIC, MAX-DOAS BIRA) show quite similar diurnal variations with increasing NO₂ in the morning, a maximum around 12 KST, and a decrease towards the evening. In general, this aligns with previous studies, which found up to 40 % reduction of NO₂ columns in the OMI afternoon overpass compared to the SCIAMACHY morning over urban regions (Boersma et al., 2008, 2009) and similar reductions using GOME-2 morning and OMI afternoon observations over large urban regions in the US (Penn and Holloway, 2020). However, the GEMS observations reveal that the morning observations of SCIAMACHY and GOME-2 are in the increasing part, while the afternoon observations of OMI are in the decreasing part, and the maximum of NO₂ in Seoul around 12 KST is in between and not captured by previous missions. The data sets at the Pandora Yonsei site and observations are also visible for the GEMS L2 product (see Appendix Fig. A7), but less pronounced as it is generally high biased. These differences for observations at larger SZA can be explained by a lower sensitivity and more uncertain AMFs for these scenes, which is amplified for larger aerosol loads and low boundary layer heights in combination with a lack of knowledge of the tropospheric aerosol in the MAX-DOAS UB Incheon, which already is at the edge of the SMA, show less diurnal variation with an earlier maximum around 11 KST, a slight decrease, and more of a plateau in the afternoon. The less polluted sites show little diurnal variability. For the Pandora Seosan site, the NO₂ slightly decreases over the day towards the evening. For the Pandora Ulsan site, on the other hand, NO₂ increases slightly over the day. Interpreting these observed differences in diurnal variability is difficult as they are driven by emissions, chemistry of NO_x, and transport processes. These driving factors vary with season, wind speed, transport processes, and weekday-weekend effects, which are analyzed in more detail in the following sections.

5.2 Seasonality

Figure 6 shows the diurnal variability divided into winter (DJF), spring (MAM), summer (JJA), and autumn (SON) from the AMF calculation for the GEMS IUP-UB and the station's data sets for those stations which were operated over the whole year. Diurnal variability of median tropospheric NO₂ VCDs from the GEMS IUP-UB product (blue) and ground-based stations (red) for the individual seasons (DJF, MAM, JJA, SON). The TROPOMI observation is added in black. Station names can be found in the individual titles. Error bars represent the 25 and 75 % quantiles of the MAX-DOAS and GEMS observations. In general, NO₂ values are higher in winter than in summer. For product. This is further discussed in Sect. 5.4. During the summer months (JJA), several the polluted stations (MAX-DOAS UB Incheon, Pandora Yonsei, Pandora SNUSeoul) show a minimum in the NO₂ VCDs around noon (around 13 KST). Similar consistent results were found by Yang et al. (2024) and Edwards et al. (2024). This observation would fit the expectation that chemical loss is strong relatively rapid during noon, especially in summer, and significantly influences the diurnal variability variation of NO₂. However, this summer noon mini-

mum is more pronounced in the stationary observations than in the GEMS IUP-UB columns, which show ~~less a smaller~~ diurnal variation. Due to low data availability during the summer months in the GEMS L2 product after quality and cloud filtering, it is difficult to determine if this behavior is also present in the GEMS L2 observations.

Based on the ~~less significant role of NO_x chemistry reduced chemical loss of NO₂~~ during winter time and expected higher emissions, one would expect an accumulation of NO₂ and increasing tropospheric NO₂ VCDs over the day. This was also seen by ~~Yang et al. (2023b) Yang et al. (2024)~~ for total column observations of GEMS ~~and two Pandoras in Beijing and Seoul, for the Pandora in Beijing, and the Pandora Seoul but not for Pandora Yonsei.~~ However, this is not visible for the ~~five six~~ sites analyzed here. On the contrary, the observed tropospheric NO₂ VCDs tend to decrease over the day. ~~Most variation over the day is visible for~~ This is also visible for the GEMS L2 product in the Appendix Fig. A7.

~~The largest diurnal variation of tropospheric NO₂ VCDs are observed in~~ spring and autumn ~~months.~~ During these seasons, the ~~polluted stations in the SMA show quite similar diurnal variation with increasing NO₂ follows the described variability with an increase during the in the~~ morning, a maximum ~~at late morning, respectively noon close to noon~~ around 11/12 KST, and a decrease towards the ~~afternoon. Since these months have the highest data availability, they are dominating the diurnal variability averaged over the whole observation period, seen in Fig. ??.~~ Differences between the GEMS IUP-UB ~~evening.~~ This agrees

~~with previous studies, which found up to 40 % reduction of NO₂ columns in the OMI afternoon overpass compared to the SCIAMACHY morning over urban regions (Boersma et al., 2008, 2009) and similar reductions using GOME-2 morning and OMI afternoon observations over large urban regions in the US (Penn and Holloway, 2020). Also Edwards et al. (2024) showed that GEMS tropospheric NO₂ VCD variation can be large, especially in polluted environments (>50 % of the tropospheric VCD). However, the GEMS observations reveal that for the SMA the morning observations of SCIAMACHY and GOME-2~~

~~are in a period where tropospheric NO₂ is increasing, while the afternoon observations of OMI are in the period where the tropospheric NO₂ VCD is decreasing, and the station columns differ between seasons and sites. For the Pandora SNU site, maximum of NO₂ in the SMA around noon is in between and not captured by previous missions.~~

If observations are averaged for a full year, the diurnal variation is distorted by the early and late data coming from the summer observations only because there are no scans in winter during these times. Deviations are largest in the early morning and late

~~afternoon observations, which are for Korea available only from April to September. The diurnal variation of the median relative differences for the different seasons is shown in the Appendix Fig. A9. The diurnal variation of the deviations is similar over the seasons. However, the GEMS IUP-UB product overestimates the station columns in autumn, but both show very similar diurnal variability. In summer, on the other hand, the GEMS IUP-UB product underestimates the station columns, especially in the morning and afternoon. A similar behavior is visible for the MAX-DOAS UB Incheon and Pandora Yonsei sites. The Pandora Seosan site shows the overestimation of the GEMS IUP-UB product, already seen in the overall diurnal variation plot, in all seasons. The differences seen for the Pandora Busan site in the late afternoon are dominated by the spring and summer observations. These differences IUP-UB summer observations show a larger negative bias during summer. Due to the limited number of sites and observations available in summer, further investigation is needed The median relative differences at the individual sites~~ are also summarized in a heatmap ~~plot in time series plot in the Appendix Fig. A8, showing an underestimation~~

~~of the GEMS IUP-UB compared to the station tropospheric NO₂ VCDs in blue and overestimation in red. Time series of~~

the median relative differences at the different ground-based sites from 1 October 2021 to 31 October 2022. The stations are ordered from bottom to top by increasing median ground-based tropospheric VCD. In general, no overall seasonality of the biases is visible. For the Pandora SNU-Seoul site, the discussed positive bias is visible for the autumn and winter observations. For the Pandora Busan site, the GEMS IUP-UB product overestimates from the beginning of January to the beginning of March while having mostly negative biases for the rest of the year. Additionally, the already discussed overall positive bias for the Pandora Ulsan and Seosan sites is visible, which seems to be a bit more pronounced in spring observations and needs to be further investigated.

5.2 Effects of wind speed and transport processes

Figure 7 and Fig. 8 illustrate the sensitivity of the diurnal variability of variation of the tropospheric NO₂ VCDs to wind speed. Observations are separated into calm (wind speeds < 3 ms⁻¹, Fig. 7) and windy (wind speeds ≥ 3 ms⁻¹, Fig. 8) conditions based on ERA5 10 m wind data (Hersbach et al., 2023), temporally and spatially interpolated to the GEMS observations. Due to reduced data availability after the separation, only selected sites are shown. The diurnal variability is quite different for calm and windy conditions for some of the shown sites and seasons but consistent for the GEMS IUP-UB and the ground-based data. However, the agreement is better for windy conditions than for low wind speeds, which can be explained by more increased dispersion during windy conditions, resulting in less fewer inhomogeneities. For calm conditions,

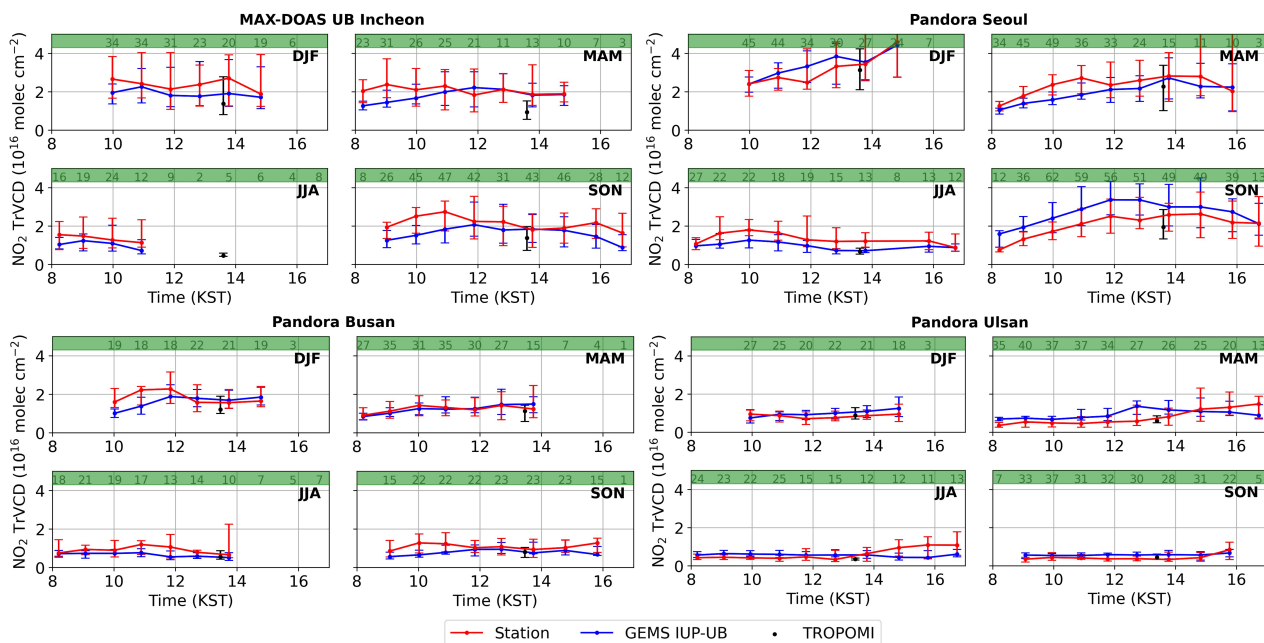


Figure 7. Same as Fig. 6 but only including observations-tropospheric NO₂ VCDs with wind speeds < 3 ms⁻¹ for selected sites with still good data availability.

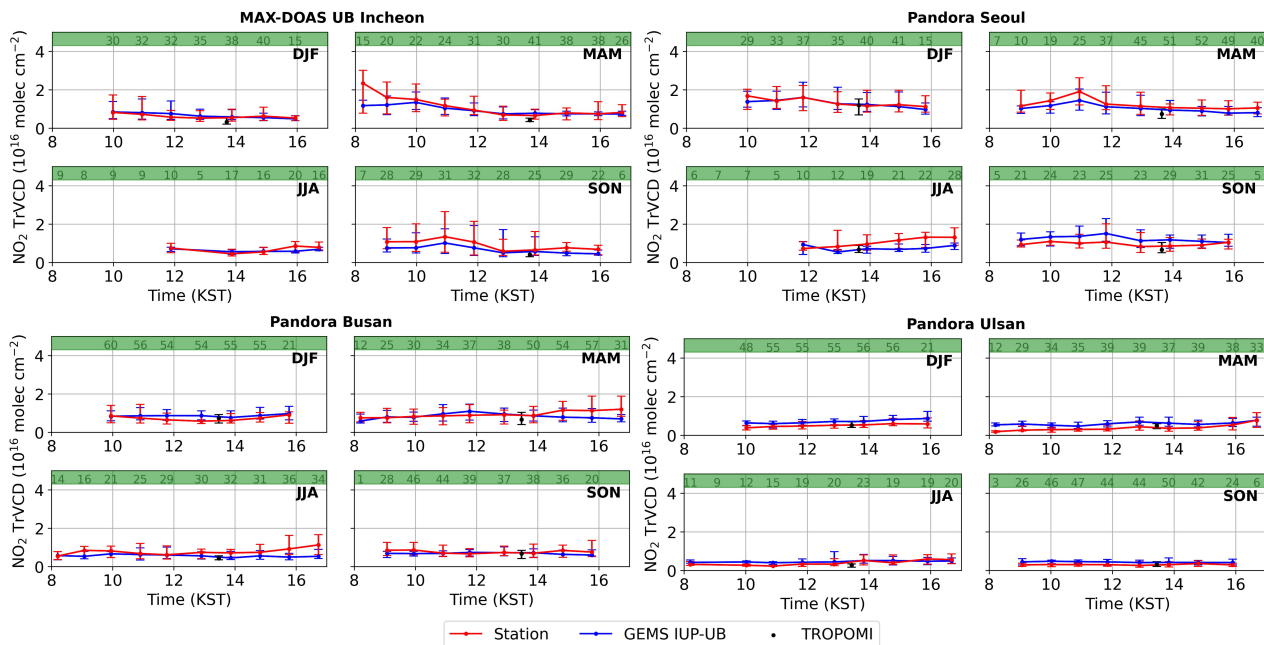


Figure 8. Same as Fig. 6 but only including observations-tropospheric NO₂ VCDs with wind speeds $\geq 3\text{ms}^{-1}$ for selected sites with still good data availability.

the tropospheric NO₂ columns-VCDs are generally larger due to accumulation of emissionsthe accumulation of local emissions (see also Chong et al. (2018)). For windy conditions, the observations show much less variability-variation over the day because emissions are dispersed quickly. Differences between calm and windy conditions are smaller for the less polluted sites. Largest-At the Busan site, the Pandora data show an increase of NO₂ during the afternoon in spring and summer for windy conditions (Fig. 8). Which is not captured by GEMS and is not visible during calm conditions. This increase might be explained by local transport effects, which move NO₂ in the line of sight of the Pandora with the wind changing to southerly directions in the afternoon (see Fig. 9).

The largest differences between calm and windy conditions and between the seasons are found for the Pandora SNUSeoul, the most polluted site of the four. During calm days in winter, the NO₂ shows a strong increase over the day. This can be attributed to the less effective chemical loss in winter and the accumulation of emissions that cannot be balanced by dilution on calm days. This increase over the day in winter was also shown based on GEMS total NO₂ columns by Yang et al. (2023b) but already when considering all data Yang et al. (2024). Yang et al. (2024) saw this increase already for all winter data without a wind filter, which is not visible in our tropospheric NO₂ VCD data set. After filtering for windy only low wind conditions they observed an even stronger increase. For spring and autumn, the NO₂ increases in the morning, decreases-starts decreasing again around noon and flattens out in the afternoon. During summer, when the chemical loss is even more effective, the minimum is around noon, but in general, there is less variabilityvariation.

Differences between calm and windy conditions are smaller for the less polluted sites. The Pandora SNU is the only site showing a strong increase over the day in winter during calm conditions. Interestingly, a significant increase is visible in the tropospheric NO₂ VCDs for the Pandora Ulsan site observations in spring during low wind speeds. Similar also during summer but then not captured by GEMS. The increase is not happening over the whole day but starting around noon. This, slightly later for the station data. This increase can be explained by transport effects, as illustrated by Fig. 9. Chong et al. (2018) observed similar transport effects for other remote Pandora sites close to emission sources during the Megacity Air Pollution Studies-Seoul (MAPS-Seoul) campaign from May to June 2015. This kind of transport effects can now be better followed and understood by the hourly maps of tropospheric NO₂ VCD observation provided by GEMS observations. Figure 9 shows maps of GEMS IUP-UB tropospheric NO₂ VCDs averaged for May 2022 for each of the ten observations per day. Overlaid are the interpolated ERA5 10 m wind data. The maps show the southeast of South Korea, including the sites of the Pandora Busan, the MAX-DOAS MPIC Busan, the Pandora Ulsan, and the MAX-DOAS Ulsan. Maps

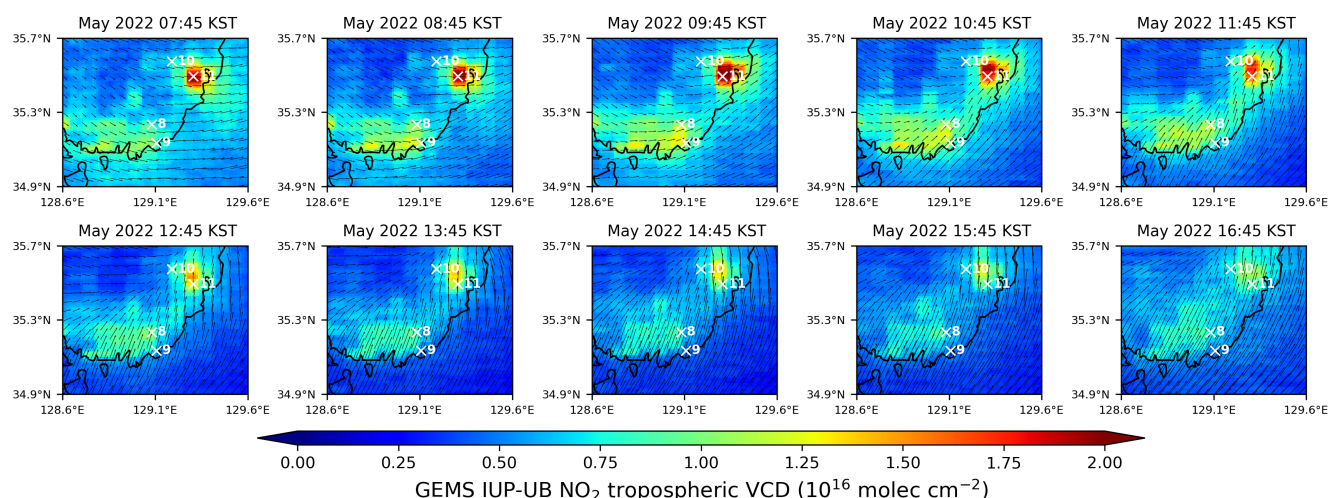


Figure 9. Maps of GEMS IUP-UB tropospheric NO₂ VCDs for the ten observations per day averaged for May 2022 overlaid with ERA5 10 m wind data. Arrow lengths indicate wind speed, and their orientation represents wind direction. Maps show the southeast of South Korea, including the sites of the Pandora Busan (8), the MAX-DOAS MPIC Busan (9), the Pandora Ulsan (10), and the MAX-DOAS Ulsan (11). Hourly monthly averaged maps for the SMA are shown in the Appendix Fig. A10

of GEMS IUP-UB tropospheric NO₂ VCDs for the ten observations per day averaged for April 2022 overlaid with ERA5 10 m wind data. Maps show the SMA, including the sites of the MAX-DOAS IUP-UB Incheon (1), Pandora Yonsei (2), Pandora SNU (3), MAX-DOAS BIRA Seoul (4), MAX-DOAS MPIC Seoul (5), MAX-DOAS BIRA Suwon (6), and Pandora Seosan (7). The GEMS IUP-UB NO₂ columns are highest for in the late morning observations and are decreasing towards the evening. Interesting is the varying. The location of the NO₂ maximum varies over the day, clearly visible along the coastline and from its location relative to the station sites. In the early morning, the NO₂ is mainly located at the MAX-DOAS UB Ulsan site. With the wind turning from mainly westerly in the morning to mainly southerly winds around noon, the NO₂ is moving northwards.

610 Therefore, the NO₂ is moving closer to the Pandora Ulsan site, which can ~~probably~~ explain the increase starting around noon visible in the spring diurnal variation plot. ~~Figure A10 illustrates a similar variation~~ Hourly monthly averaged maps for the SMA. ~~The maps show the GEMS IUP-UB tropospheric~~ showing the NO₂ VCDs averaged for the ten observation times per day for April 2022 over the SMA with overlaid ERA5 wind data. ~~The GEMS IUP-UB NO₂ columns are increasing~~ build-up during the morning, ~~reaching their maximum for the 10:45 KST observation, and are decreasing towards the evening.~~ While in the early morning, the NO₂ is concentrated over the SMA's central part with most of the instruments, it is moving eastwards, with the wind direction turning from easterly low wind speeds to strong westerly winds. For the 12:45 and 13:45 KST observations, the NO₂ hot spot is located east of the Pandora Yonsei and SNU sites transport over the day are shown in the Appendix Fig. A10.

~~Additionally~~ In addition to the diurnal ~~variability~~ variation of transport effects due to changing wind direction, Fig. 10 illustrates ~~also~~ the seasonal variability. Shown are maps of monthly averaged GEMS IUP-UB tropospheric NO₂ VCDs for the 13:45 KST observation from October 2021 to September 2022 for the southeast of South Korea, with overlaid ERA5 10 m wind data. The GEMS IUP-UB NO₂ columns are highest from late autumn to early spring and have their minimum during the summer months. From September to January, with a mainly northwesterly wind direction, a large part of the NO₂ is located over the ocean and mostly south of the ground-based stations. During spring, when the wind is changing from northwest to mostly southwest, the NO₂ is moving northwards.

The described influences of wind speed, causing dispersion or accumulation, and transport effects due to varying wind directions over the day and the year, complicate the interpretation of observed diurnal variations of tropospheric NO₂ VCDs in terms of emissions and chemistry.

5.3 Weekday-weekend effect

630 Another influence on the diurnal variation of NO₂ is the difference in emissions ~~for on~~ working days and ~~weekends~~ those on weekends (Beirle et al., 2003; Stavrou et al., 2020, e.g.). Figure 11 shows the tropospheric NO₂ VCDs of the day of the week normalized with the mean NO₂ from Monday to Friday for the GEMS IUP-UBL2, the GEMS L2IUP-UB, and the TROPOMI observations with the collocated station observations. GEMS observations are averaged over all available observations per day. TROPOMI observations are only available once or twice a day in cloud-free conditions. Therefore, some deviations between the TROPOMI and GEMS ~~observations can be explained due to~~ tropospheric NO₂ VCD are explained by the reduced data availability ~~or and~~ the timing effect. Due to different sampling ~~for of~~ the three satellite products, each has its own coincident stationary data set.

Generally, there is a good agreement between the respective satellite products and their corresponding ground-based measurements. Similarly, there is ~~a~~ good agreement among the different NO₂ products, with a few exceptions, mainly caused by the sparse TROPOMI observations. During the weekdays, from Monday to Friday, most normalized VCDs are close to one. Already on Saturday, the NO₂ is reduced compared to the weekdays. On Sundays, the NO₂ is reduced between around 20 % and 50 % compared to the average observed on weekdays. This reduction is significantly larger than the 10-20 % found in studies based on OMI and GOME data over Seoul (Beirle et al., 2003; Stavrou et al., 2020). The smallest decline over the

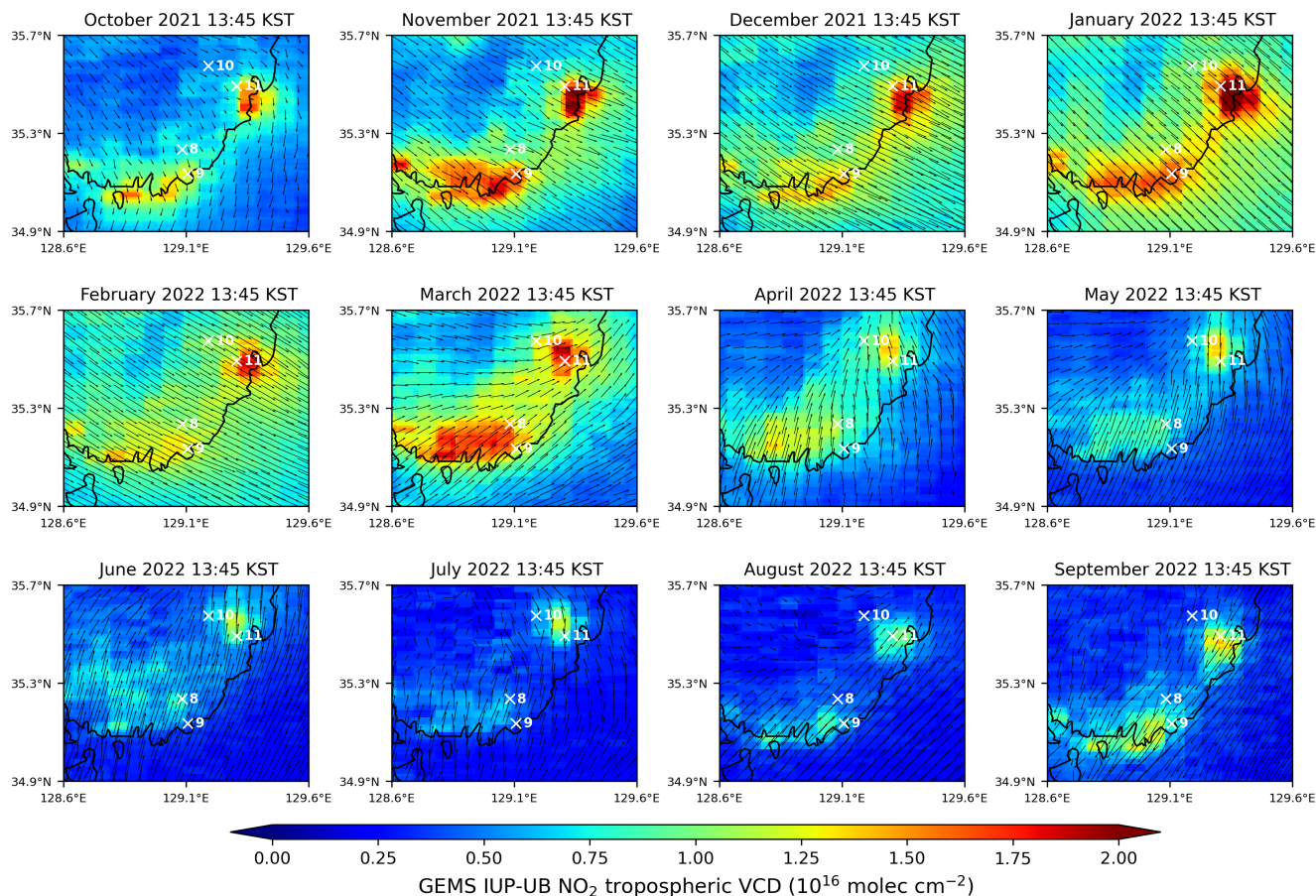


Figure 10. Maps of monthly averaged GEMS IUP-UB tropospheric NO₂ VCDs for the 13:45 KST observation from October 2021 to September 2022 overlaid with [averaged ERA5 10 m wind data](#). [Arrow lengths indicate wind speed, and their orientation represents wind direction](#). Maps show the southeast of South Korea, including the sites of the Pandora Busan (8), the MAX-DOAS MPIC Busan (9), the Pandora Ulsan (10), and the MAX-DOAS Ulsan (11).

weekend is observed in Seosan, a more remote [station site](#) with less influence [of from](#) traffic emissions. [For some sites, NO₂ is already reduced on Fridays, i.e., Pandora Busan.](#) MAX-DOAS BIRA Seoul and MAX-DOAS MPIC Seoul [are, for example,](#) both located in Seoul, still show some differences. NO₂ at the MAX-DOAS BIRA Seoul site peaks on Fridays and shows similarly strong reductions on Saturdays and Sundays, while at MAX-DOAS MPIC Seoul NO₂ peaks on Thursdays, and the reductions [start Friday and](#) are strongest on Sundays. This could be due to local differences but also to [the slightly](#) different months in which the stations are operated and the data analyzed. Large differences in the TROPOMI observations compared to the GEMS observations, e.g., Fridays for the MAX-DOAS BIRA Seoul site, [could can](#) be explained by the different sampling with observations between 12:28 KST, and 14:37 KST, which might be biased to certain weeks or months because of cloud cover.

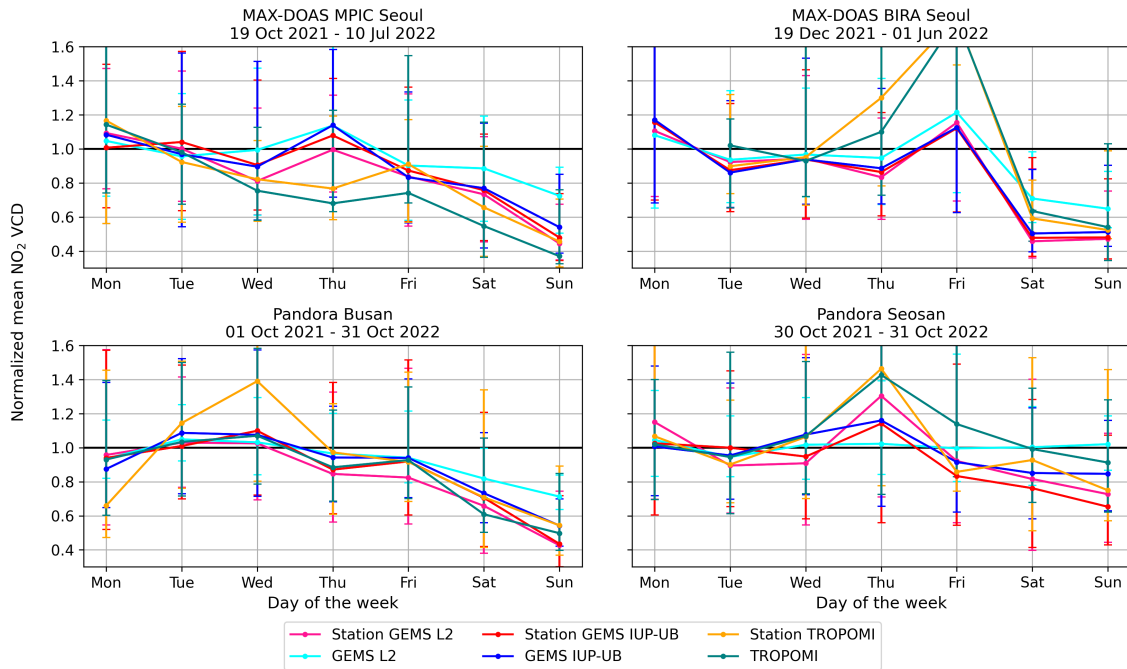


Figure 11. Plots of normalized weekday tropospheric NO₂ VCDs for the co-located station observations with the GEMS IUP-UB-L2 (bluecyan), the GEMS L2-IUP-UB (cyanblue), and the TROPOMI (turquoise) observations. The corresponding station measurements are marked in pink for the GEMS L2 product, in red for the GEMS IUP-UB product, and in yellow for the TROPOMI product. Station names and operation periods can be found in the individual titles. [More sites are shown in the Appendix Fig. A11](#)

655 **Interesting to see is the deviation of the The GEMS L2 product on weekends shows a distinct deviation on the weekend.** The agreement with the other data sets is very good during the weekdays, but on Saturday and Sunday, there is less reduction compared to the average observed on weekdays than for the other products. One possible explanation is the in general higher background NO₂ values in the GEMS L2 product, which do not have a weekly cycle. **Plots of the diurnal variability on the weekend and weekdays from the tropospheric NO₂ VCDs of the GEMS IUP-UB product and the ground-based stations can be found in the Appendix Fig. ??.**

5.4 Discussion of GEMS - ground-based deviations

660 The agreement between the GEMS IUP-UB and the ground-based observations is already very promising. However, possible explanations for observed differences have to be discussed.

One potential reason for deviations between the GEMS and ground-based observations could be a poor stratospheric correction. Since the contribution of the stratosphere is small with column densities in the order of $10^{14} \text{ molec cm}^{-2}$ to $10^{15} \text{ molec cm}^{-2}$, especially compared to the typically observed tropospheric NO₂ VCDs in the range of $10^{16} \text{ molec cm}^{-2}$, it up to $1 \times 10^{17} \text{ molec cm}^{-2}$. **the influence** is not very likely large. However, under some conditions, the operational GEMS product has a large bias in the

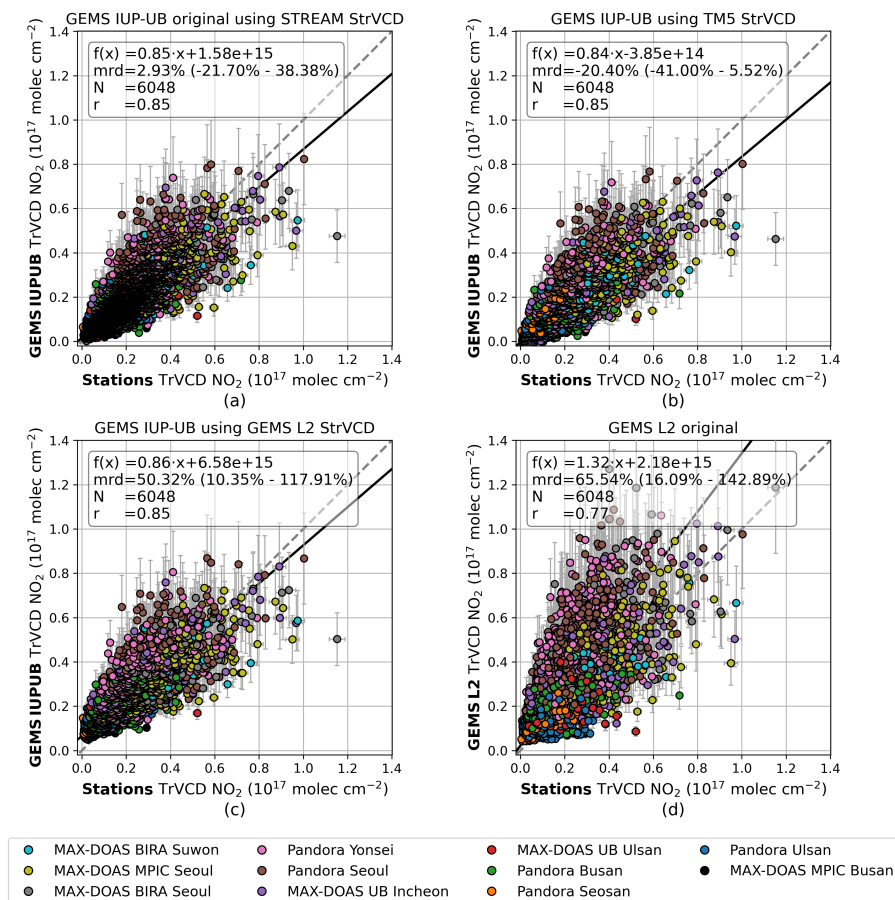


Figure 12. Scatter plots of satellite vs. co-located ground-based NO₂ tropospheric VCDs; for (a) the original GEMS IUP-UB product using the STREAM-based stratospheric VCDs, (b) the GEMS IUP-UB using the TM5 stratospheric VCDs, (c) the GEMS IUP-UB using the GEMS L2 stratospheric VCDs, and (d) the original GEMS L2 product.

stratospheric columns, and in such situations, the stratospheric correction can be a significant source of error. To investigate the influence of the different stratospheric VCD products, subversions of the GEMS IUP-UB product, using different stratospheric column products, were created. Figure 12 shows scatter plots of coincident satellite and ground-based tropospheric NO₂ VCDs for (a) the original GEMS IUP-UB product using the STREAM-based stratospheric VCDs, (b) the GEMS IUP-UB using the TM5 stratospheric VCDs, (c) the GEMS IUP-UB using the GEMS L2 stratospheric VCDs, and (d) the original GEMS L2 product. Replacing the STREAM-based stratospheric VCDs with the TM5 stratospheric VCDs increases the bias from 3% (-22% - 38%) to -20% (-41% - 5%) and changes the offset from $+1.6 \times 10^{15}$ molec cm⁻² to -3.9×10^{14} molec cm⁻². This illustrates that the TM5 model stratospheric VCDs are too large, resulting in too low and even negative tropospheric NO₂ VCDs in the GEMS IUP-UB retrieval. Using the GEMS L2 stratospheric VCDs for the GEMS IUP-UB product, increases the bias and the offset, illustrating that the GEMS L2 stratospheric VCD product is too low. This results in an overestimation of

the GEMS IUP-UB tropospheric NO₂ VCD compared to the station data. The correlation stays constant for both subversions as there is little correlation between the stratospheric NO₂ columns and the tropospheric NO₂ variations at the stations. The larger scatter in the operational GEMS L2 product is investigated in the following. The diurnal variation of the stratospheric NO₂ VCD products is shown in the Appendix Fig. A12. As expected, the TM5 model stratospheric VCDs, which are used for the TROPOMI product, agree well with the TROPOMI stratospheric NO₂ VCD value. The GEMS IUP-UB STREAM-based stratospheric columns show a very similar diurnal evolution as the TM5 data but are slightly lower. The GEMS L2 product shows a similar but slightly less variation over the day and is lower by a factor of around 2.5 when compared to the TM5 and GEMS IUP-UB stratospheric columns.

Another explanation for deviations between the GEMS and ground-based observations could be the effect of the Bidirectional Reflectance Distribution Function (BRDF), especially for the observations of diurnal evolution. However, the GEMS L2 product considers the BRDF influence using GEMS reflectivity data, yet the discrepancy with the ground-based data remains. To investigate the BRDF effect on the GEMS IUP-UB product, we replaced the TROPOMI LER product, used in the GEMS IUP-UB product, with the GEMS L2 reflectivity. Figure 13 shows the scatter plots of (a) the GEMS L2 product using the GEMS L2 reflectivity in the AMF calculation, (b) the GEMS IUP-UB product using the TROPOMI LER reflectivity, both analyzed before, and (c) the modified GEMS IUP-UB product using the GEMS L2 reflectivity. The modified GEMS IUP-UB product

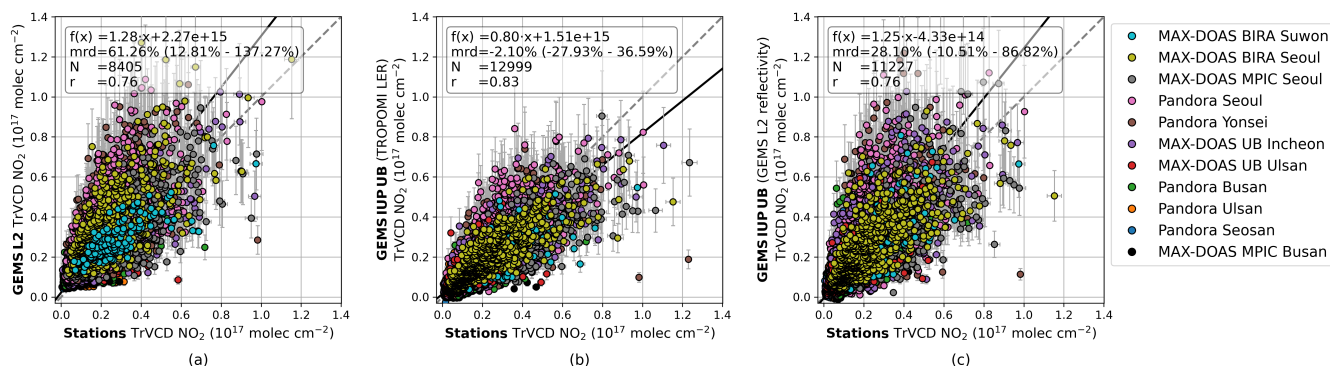


Figure 13. Scatter plots of satellite vs. co-located ground-based NO₂ tropospheric VCDs. For: for (a) the GEMS L2 product using the GEMS L2 reflectivity in the AMF calculation, (b) the GEMS IUP-UB product using the TROPOMI LER reflectivity, and (c) the GEMS IUP-UB product using the GEMS L2 reflectivity.

shows more scatter than the original version and an overestimation similar to the GEMS L2 product, indicating that the GEMS reflectivity causes a large part of the overestimation and scatter.

Discrepancies between the MAX-DOAS and GEMS IUP-UB observations could be explained by the used model profiles. With its resolution of $1^\circ \times 1^\circ$, the TM5 model has a rather poor spatial resolution compared to the GEMS pixel size and the spatial variability of NO₂. Furthermore, it should be noted that the TM5 model has no specific focus on the GEMS region. Yang et al. (2023a) demonstrates that an updated version of the GEOS-Chem standard model with a resolution of $0.25^\circ \times 0.3125^\circ$ well reproduces diurnal variation of NO₂ vertical mixing observed during the KORUS-AQ campaign. This could be further

investigated by considering MAX-DOAS profiles and the GEMS averaging kernels. However, car DOAS measurements show that sometimes there can be large fluctuations within individual satellite pixels, and station measurements may be located in sub-pixel regions that are not representative of the entire pixel.

Another already mentioned aspect ~~possibly contributing~~, which possibly contributes to the differences, especially at larger SZA, is the lack of knowledge of tropospheric aerosol in the calculation of the AMF for the GEMS IUP-UB product. However, the L2 product considers aerosol parameters from GEMS observations in the AMF determination and should be correct for their influence. The expected improvement is not reflected in the comparisons.

Due to less sensitivity at higher SZA (and VAA), AMFs are expected to be more uncertain for these scenes. This uncertainty is further enhanced for larger aerosol loads and with low boundary layer heights in the morning and evening.

6 Summary and conclusions

We In this study we evaluated tropospheric NO₂ VCDs of the operational GEMS L2 v2.0, the scientific GEMS IUP-UB v1.0, and the operational TROPOMI v02.04.00 product with ground-based DOAS observations from 11 stationary and additional mobile car DOAS instruments in South Korea. GEMS is the first instrument in geostationary orbit, enabling the observation of diurnal variations of NO₂ for over a large part of Asia. With its location centered over South Korea, GEMS provides up to 10 observations during daytime. The GEMS IUP-UB and the ground-based observations are used together with ERA5 10 m wind data to interpret the diurnal variation of tropospheric NO₂ VCDs.

Maps of tropospheric NO₂ VCDs from the GEMS L2 ~~v2.0~~, the GEMS IUP-UB, and the TROPOMI product, all around the the time of TROPOMI overpass, show the dominant large NO₂ hot spot spots over the SMA and the smaller urban agglomerations. These hot spots, especially that above the SMA, show the highest values in the GEMS L2 product. The lowest values are found in the TROPOMI product. The background tropospheric NO₂ ~~is comparable between~~ VCD is similar for the TROPOMI and the GEMS IUP-UB products but is significantly higher in the GEMS L2 product, presumably because of the different approaches used for the stratospheric correction. Due to a missing interpolation of the AMF, the GEMS L2 product shows box structures with the spatial resolution of the GEOS-Chem model.

The evaluation of the ~~three products~~ GEMS L2 v2.0 tropospheric NO₂ VCD product with the ground-based DOAS measurements ~~shows an overestimation by the GEMS L2 product~~ indicates an overestimation, with a slope of ~~1.41~~ 1.28, a median relative difference of ~~+64~~ 61 %, and a correlation of ~~0.75~~ 0.76. The evaluation results of the GEMS IUP-UB and the operational TROPOMI products ~~are comparable~~ show that both are low biased and have less scatter than the GEMS L2 product. The slope and median relative difference are ~~0.89 and -10.80 and -2~~ % for the GEMS IUP-UB product and 0.79 and ~~-14~~ -16 % for the TROPOMI product. The correlation of the GEMS ~~IUP-UB improved from 0.82 to 0.85~~ products with the ground-based observations improves when observations are limited to the TROPOMI overpass time. ~~This brings the correlation closer to the 0.88 of the TROPOMI product~~, indicating larger deviations in coinciding morning and/or afternoon observations. ~~All comparisons between satellite and ground-based observations are based on the closest pixel within a radius of 5 km around the station site. Other co-location criteria with different distances, averaging satellite data around the station area and considering~~

~~the viewing direction dependency have not significantly improved the comparisons.~~ The separate comparison of the satellite and ground-based ~~observations~~ tropospheric NO₂ VCDs for the 11 individual sites illustrates some differences ~~in agreement~~ between the sites. ~~Correlation for the GEMS IUP-UB product varies between 0.67 for the MAX-DOAS IUP-UB Ulsan site and 0.87 for the MAX-DOAS IUP-UB Incheon site. The slope varies between 0.40 for the MAX-DOAS MPIC Busan site and 1.17 for the Pandora SNU at Seoul National University (SNU).~~ Biases are larger for more polluted sites, while less polluted sites show differences ~~elose~~ closer to zero. The positive bias for the two least polluted sites is probably related to the stratospheric correction in the GEMS IUP-UB product. In general, the GEMS IUP-UB product and the TROPOMI product show good agreement in the individual biases, ~~supporting the good agreement visible in the overall comparison.~~ Mobile car DOAS observations serve as an additional data set to evaluate the GEMS observations and support the results obtained from the comparisons with stationary ground-based data.

Due to the locations of the stations in different pollution regimes, the observed diurnal variations of the tropospheric NO₂ ~~columns~~ VCDs from the GEMS IUP-UB and the ground-based data sets show ~~significantly~~ different characteristics. Urban sites often show a maximum of NO₂ of varying degrees around 10/11 local time, while more rural sites show nearly no diurnal ~~variability~~ variation. For both cases, we find good agreement between the diurnal ~~variability~~ variation of the GEMS IUP-UB and the ground-based NO₂ data. The largest ~~deviations~~ differences are visible in the morning and especially for the 16:45 KST observation, where the GEMS IUP-UB product often underestimates the station values. ~~The separation of the data sets into seasons shows for the polluted sites~~ During summer the polluted sites show a minimum in the tropospheric NO₂ columns VCDs around noon (13 KST), indicating the larger influence of chemical loss in summer. However, this summer noon minimum is less pronounced in the GEMS observations than in the stationary observations. Winter observations show, in general, higher NO₂ values with rather flat or slightly decreasing NO₂ over the day, which is well captured in both data sets. We see no increase over the day, as reported by other studies using total NO₂ columns in Seoul and Beijing. Most diurnal ~~variability~~ variation is found at polluted sites in spring and autumn, with an increase during the morning, a maximum late in the morning or around noon, and a decrease towards the afternoon. ~~Due to the largest data availability, these months dominate the overall diurnal cycle.~~

Diurnal ~~variability~~ variation differs significantly for low and high wind speed conditions in both the GEMS IUP-UB and the ground-based data set. However, there is better agreement during windy conditions, likely due to increased dispersion and reduced inhomogeneities. The influence of dispersion in windy conditions results in observations displaying less diurnal ~~variability~~ variation. Observations under low wind conditions show ~~strong~~ NO₂ increases over the day but only at the most polluted sites, especially during winter. This suggests that, under calm conditions, the reduced dilution and less effective chemical loss in winter are insufficient to offset the accumulating emissions. For a more rural site, the diurnal ~~variability~~ variation with increasing NO₂ values following mean wind patterns for specific seasons and times reveals the impact of transported NO₂. Due to a ~~location specific but for these months characteristic change of~~ location-specific change in wind direction around noon, which is characteristic for these months, NO₂ pollution ~~of from~~ an industrial area is transported close to the station. This is also ~~visible~~ observed in other areas and on a seasonal basis.

When analyzing the weekday-weekend effect, a good agreement is found between the different ~~products~~ tropospheric

NO₂ VCD products. Dependent on the station, the NO₂ columns are 20 to 50 % lower on Sundays compared to the weekday average. However, the GEMS L2 product which agrees with the other data sets during weekdays shows significantly less reduction on weekends. Presumably caused by the generally higher NO₂ background values in the GEMS L2 product, which do not have a weekly cycle.

770 Significant impacts of both the stratospheric correction and the surface reflectivity on the GEMS tropospheric NO₂ VCD products were found. While the GEMS L2 stratospheric VCD is too low, resulting in too high tropospheric NO₂ VCDs, the TM5 model's stratospheric VCDs, used in the TROPOMI product, are too high, resulting in too low tropospheric NO₂ VCDs, when implemented in the GEMS IUP-UB retrieval. Surface reflectivity comparisons indicate that the GEMS L2 reflectivity is a major contributor to the observed overestimation and scattering in the GEMS tropospheric NO₂ VCD product.

775 Deviations between GEMS and ground-based observations at larger SZA might be explainable by a lower sensitivity and more uncertain AMFs for these scenes, which is amplified for larger aerosol loads and low boundary layer heights in combination with a lack of knowledge of the tropospheric aerosol in the AMF calculation for the GEMS IUP-UB product. This shows the increasing importance to have good aerosol information and to include them in the AMF calculations.

Overall, our analyses revealed significant diurnal variation of NO₂. This variation is strongly site-dependent, differs between
780 polluted and less polluted sites, and has location-specific and seasonal characteristics. GEMS IUP-UB and ground-based observations are in good agreement, ~~which~~. This is promising for expanding the the extension of the analysis of diurnal variation of tropospheric NO₂ using the extensive GEMS data set in other parts of Asia. The observed diurnal variation of NO₂ offers unique insights into the chemistry and emission of NO_x as well as transport processes, but it needs to be carefully interpreted. Our analysis shows significant impacts of both the stratospheric correction and the surface reflectivity data on the GEMS
785 tropospheric NO₂ VCD products. These analyses can also help to analyze the upcoming data sets of the follow-up geostationary air quality missions such as TEMPO over North America and Sentinel-4 over Europe.

Data availability. GEMS L2 NO₂ data can be accessed at <https://nesc.nier.go.kr/en/html/cntnts/91/static/page.do> (National Institute of Environmental Research, NIER, 2023). The GEMS IUP-UB NO₂ product is available on request. TROPOMI NO₂ data are freely available via <https://s5phub.copernicus.eu/> (Sentinel-5P Pre-Operations Data Hub, last access: 21 February 2022). The data of Pandora instruments are
790 freely available from the PGN data archive (<https://pandonia-global-network.org/>, last access: 11 October 2023). The FRM4DOAS MAX-DOAS data are available on request. The ERA5 wind data are freely available from the Copernicus Climate Change (C3S) climate data store (CDS) (Hersbach et al., 2023).

Author contributions. All co-authors contributed to the campaign either as participants and instrument operators and/or during campaign preparation. AR provided the GEMS IUP-UB NO₂ data product. HL and HH provided information to the GEMS L2 NO₂ data product.
795 CF and MMF performed the MAX-DOAS data analysis. The campaign was prepared by HH, LSC, and CKS. KL performed the final data analysis and interpreted the results together with AR. KL wrote the paper with feedback and contributions from all other co-authors.

Competing interests. At least one of the (co-)authors is a member of the editorial board of Atmospheric Measurement Techniques.

Acknowledgements. We thank the National Institute of Environmental Research of South Korea for providing GEMS data, financial support (NIER-2022-04-02-037), and the excellent organization of the GMAP 2021 and SIJAQ 2022 field campaigns. We thank all participants of
800 the GMAP 2021 and SIJAQ 2022 field ~~campaign~~campaigns. The Deutsches Zentrum für Luft- und Raumfahrt (grant no. 50 EE 2204) is acknowledged for financial support. Copernicus Sentinel-5P level-2 NO₂ data are used in this study. Sentinel-5 Precursor is a European Space Agency (ESA) mission on behalf of the European Commission (EC). The TROPOMI payload is a joint development by ESA and the Netherlands Space Office (NSO). The Sentinel-5 Precursor ground-segment development has been funded by the ESA and with national contributions from the Netherlands, Germany, Belgium, and the UK. We thank PGN instrument PIs, support staff and funding for establishing
805 and maintaining the Pandora sites used in this investigation. The PGN is a bilateral project supported with funding from NASA and ESA. MMF thanks R. Spurr for the free use of VLIDORT.

Appendix A

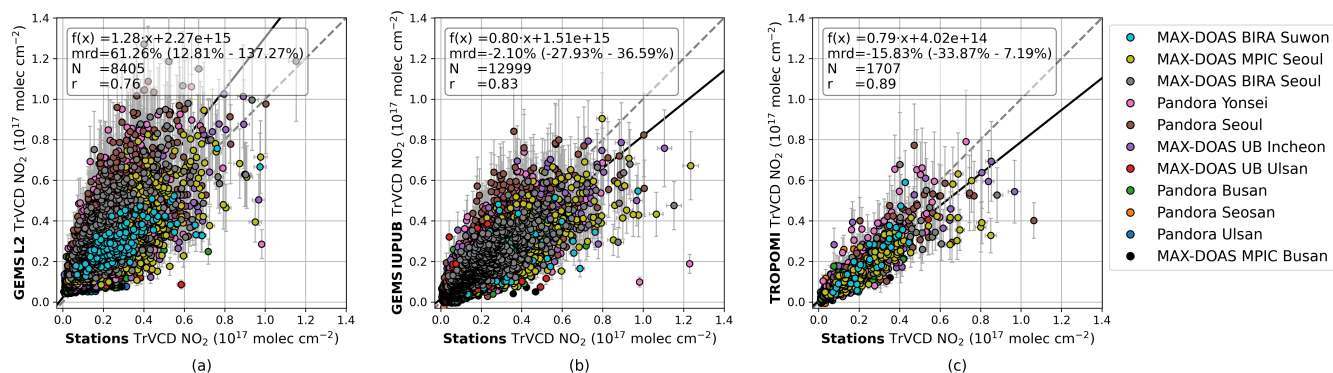


Figure A1. Same as Fig. 3 but GEMS L2 and GEMS IUP-UB observations are limited to the TROPOMI overpass time between 12:28 KST and 14:37 KST.

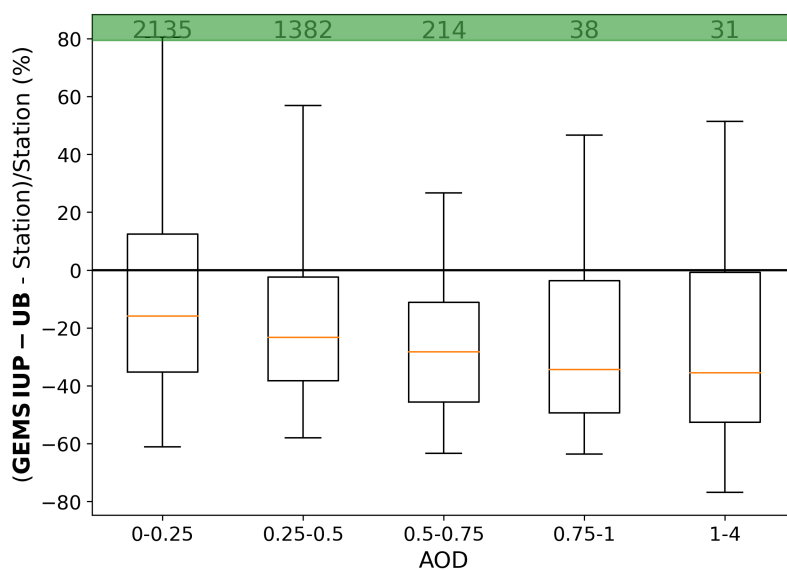


Figure A2. Relative median-Median relative differences between GEMS IUP-UB and MAX-DOAS tropospheric NO₂ columns as a function of AOD retrieved within the FRM4DOAS MAX-DOAS NO₂ analysis. Numbers in the green bar represent the number of observations contributed to the bin.

810 The comparison of satellite and ground-based observations was investigated for different spatial co-location criteria: the closest pixels within a radius of 5 km respectively 10 km around the station sites, and considering the ground-based instruments viewing azimuth angle (VAA) during satellite overpass. To investigate the VAA dependence, the GEMS pixels VCD_{sat} are weighted according to their contribution along the line of sight d of the ground-based instruments.

$$VCD_{\text{sat, VAA}} = \frac{\sum VCD_{\text{sat } i} \cdot d_i}{\sum d_i} \quad (\text{A1})$$

815 We consider the line of sight within 5 km to the station site. The comparison is only included in the analysis when more than 75 % of the line of sight is covered by satellite pixels. Measurements taken in the same VAA within the ± 20 min of the satellite observation, overlapping with the same GEMS pixels are averaged.

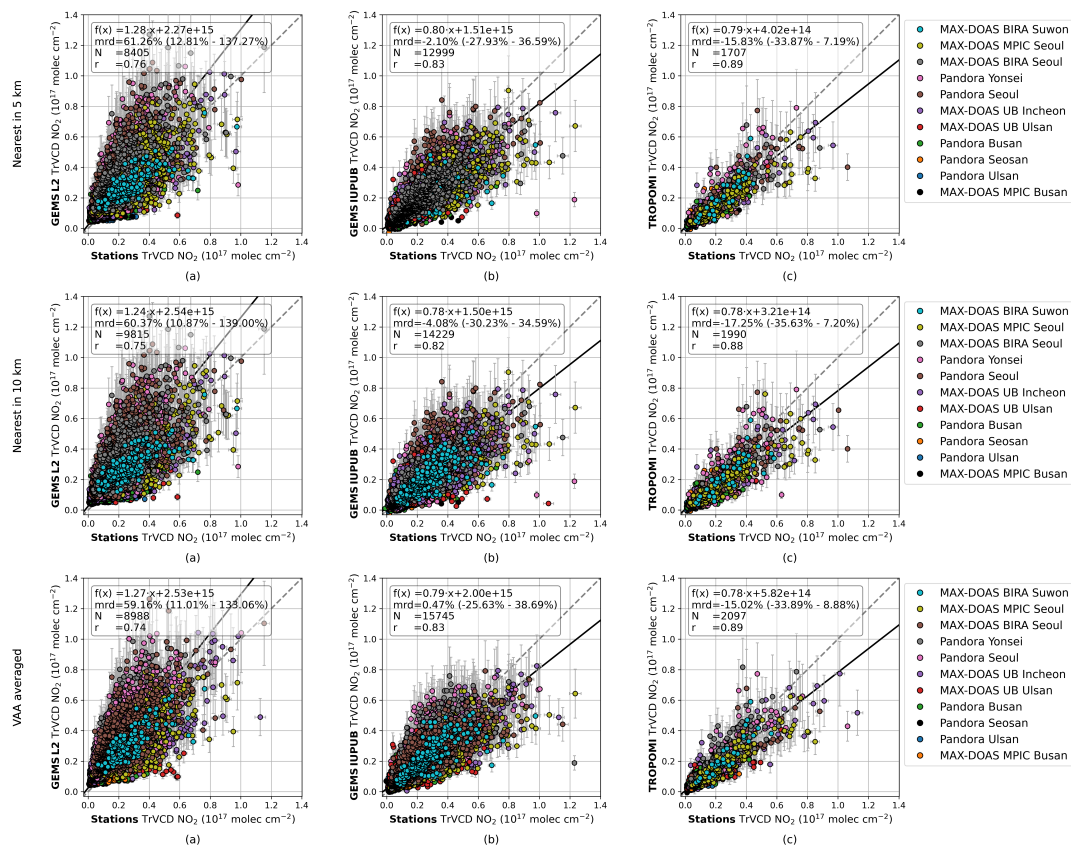


Figure A3. Scatter plots of GEMS L2 (a), GEMS IUP-UB (b), and TROPOMI (c) NO_2 tropospheric VCDs vs. co-located ground-based NO_2 tropospheric VCDs for different co-location criteria. The time constrain-constraint is with ± 20 min around the same-for-all-criteria time of the satellite measurement. First row: Ground-based-Ground-based measurements within this period are averaged and matched to the closest satellite observation within a radius of 5 km around the station site. Second row: Match to the closest satellite observation within a radius of 10 km. Third row: Satellite pixels are weighted according to their contribution along the line of sight of the ground-based instruments within 5 km of the station. Different VAA are considered independently. Fourth row: Averaging of the VAA comparisons within the ± 20 min time window.

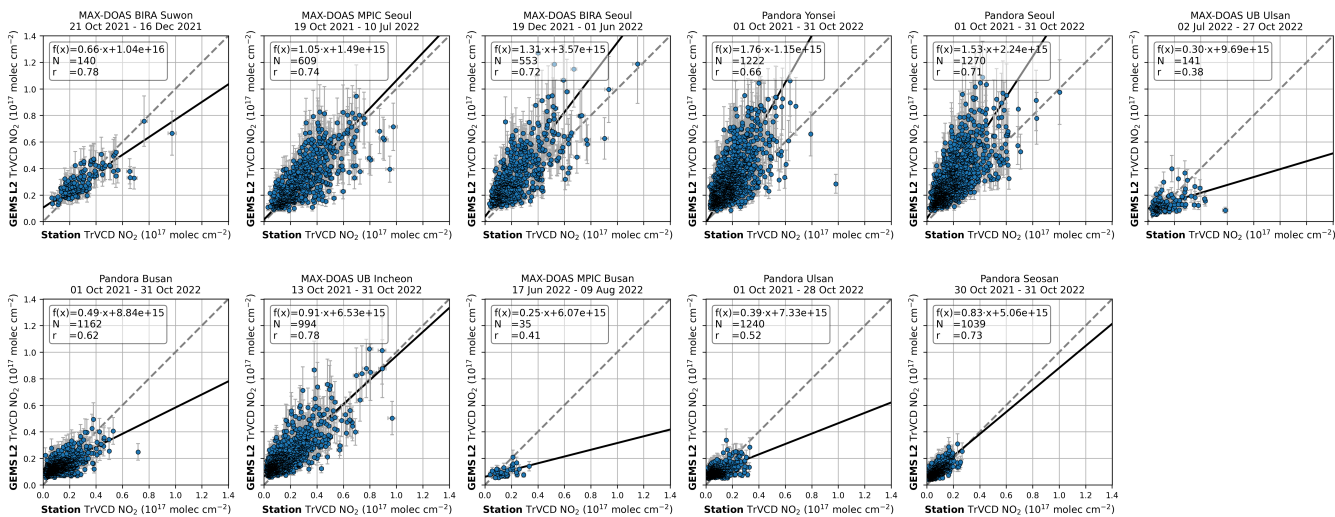


Figure A4. Same as Fig. A5 but for Scatter plots of GEMS L2 tropospheric NO₂ VCDs vs. co-located ground-based NO₂ tropospheric VCDs for the 11 individual stations. Station names and measurement periods can be found in the title. Co-location criteria are with ± 20 min and nearest 5 km the same as in Fig. 3.

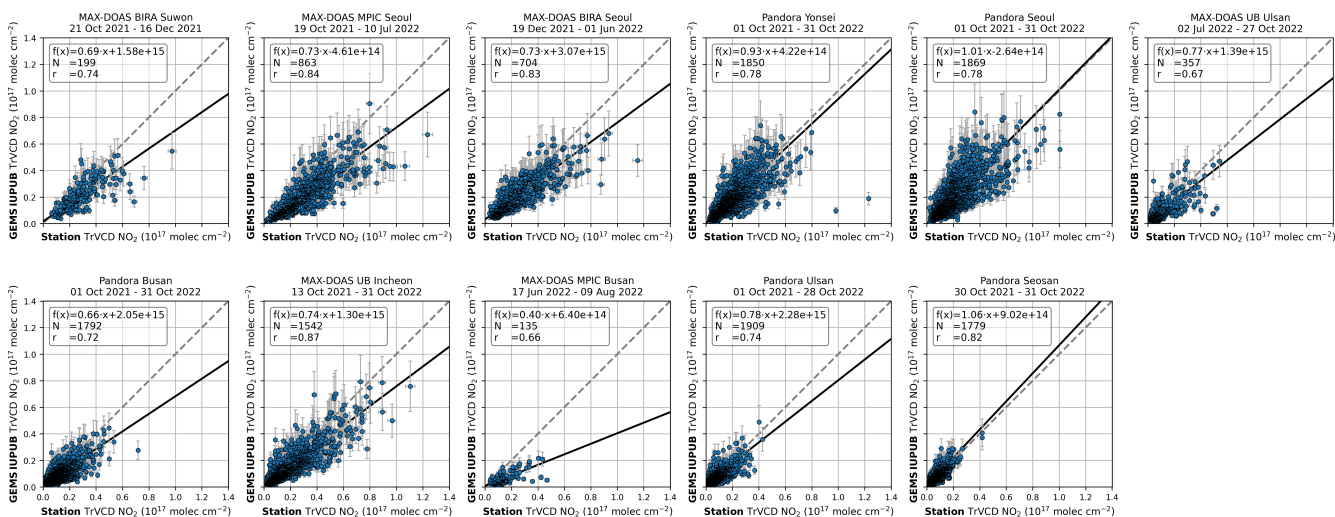


Figure A5. Same as Fig. A5 and A4 but for TROPOMI-GEMS IUP-UB tropospheric NO₂ VCDs vs. co-located ground-based NO₂ tropospheric VCDs for the 11 individual stations.

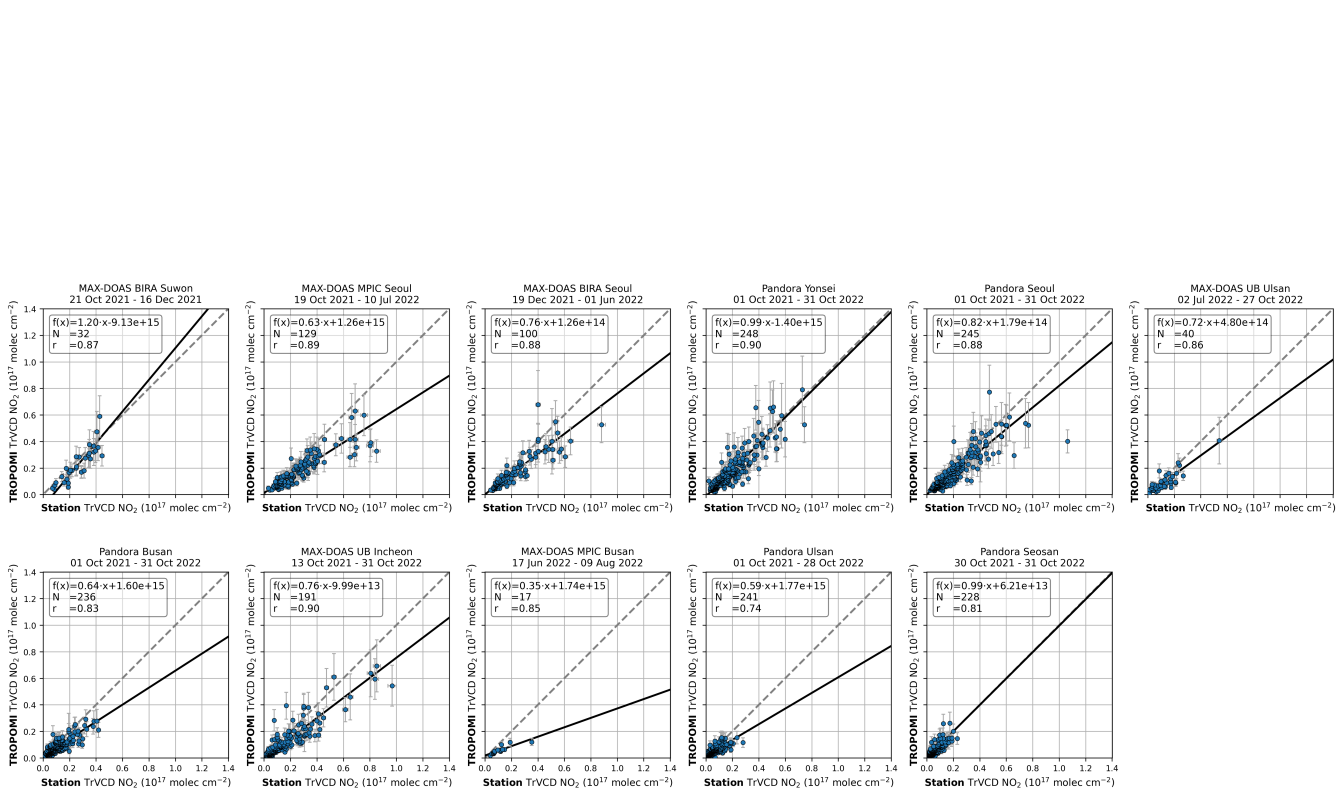


Figure A6. Same as Fig. A4 and A5 but for TROPOMI tropospheric NO₂ VCDs vs. co-located ground-based NO₂ tropospheric VCDs.

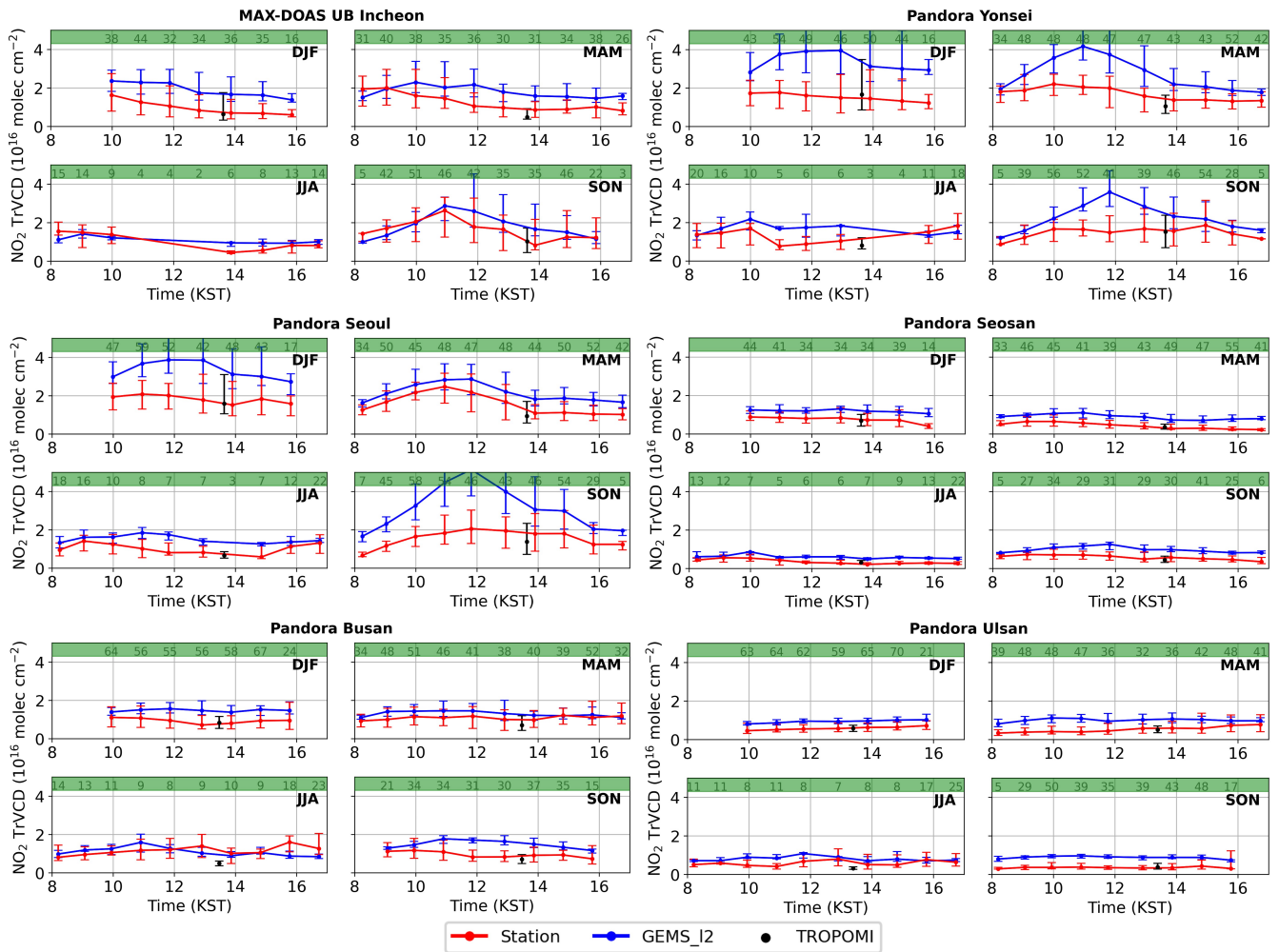


Figure A7. Same as Fig. ??-6 but for the GEMS L2 product. Diurnal variability-variation of median tropospheric NO₂ VCDs from the GEMS L2 v2.0 product (blue) and ground-based stations (red) for the individual seasons (DJF, MAM, JJA, SON). The TROPOMI observation is added in black. Station names can be found in the individual titles. Vertical bars represent the 25 and 75 % quantiles of the MAX-DOAS and GEMS observations. Due to low data availability for the GEMS L2 product in summer, observations are displayed starting at five instead of 10 available observations, see green bar.

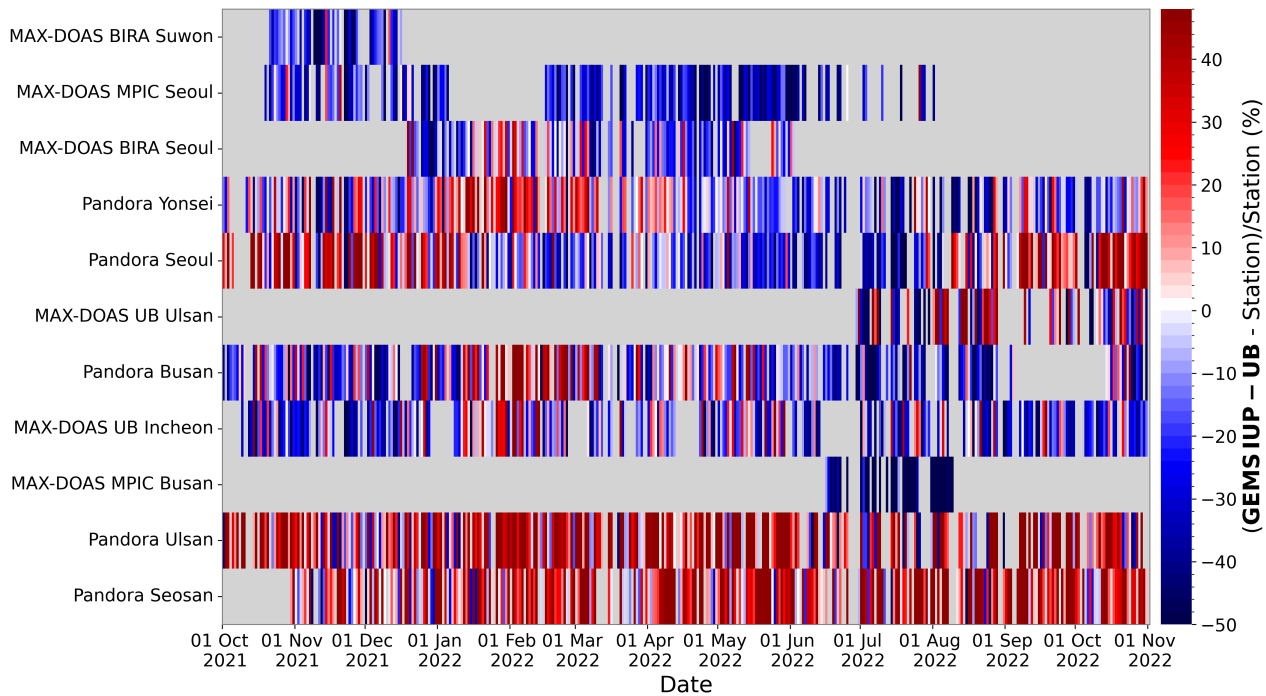


Figure A8. Same as Fig. 4 but GEMS L2 and GEMS IUP-UB observations—Time series of the median relative differences at the different ground-based sites from 1 October 2021 to 31 October 2022. The stations are limited ordered from bottom to the TROPOMI overpass time between 12:28 KST and 14:37 KST top by increasing median ground-based tropospheric VCD.

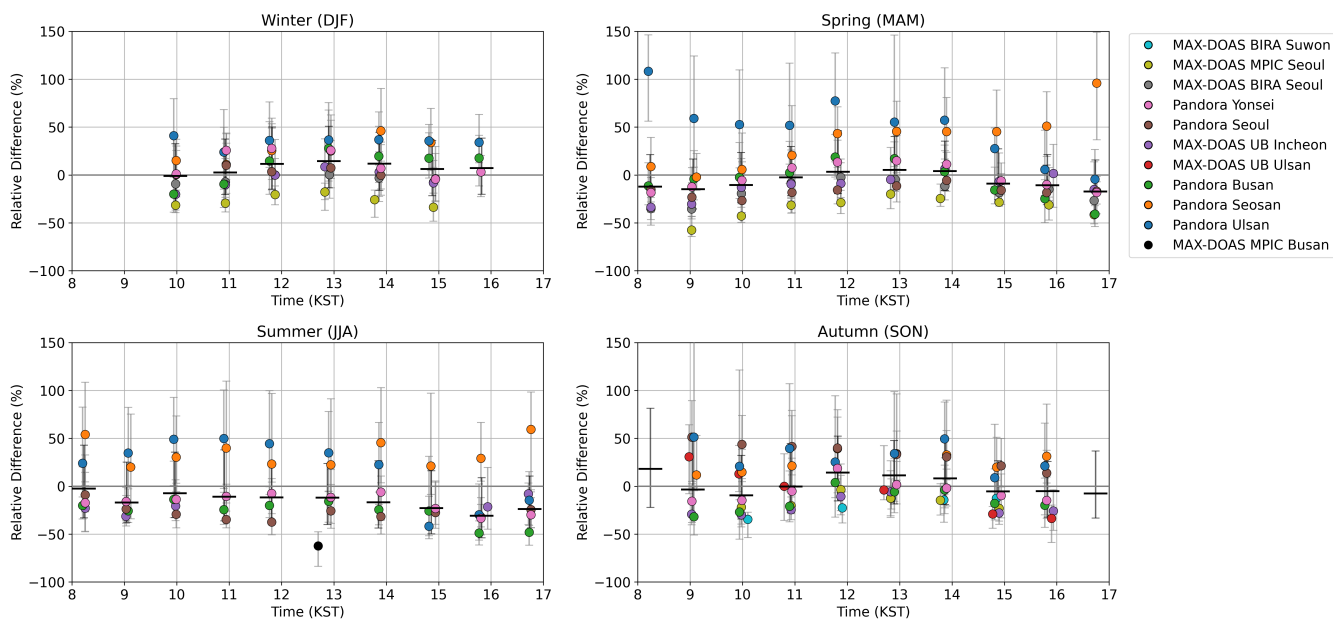


Figure A9. Diurnal variability-variation of the median tropospheric NO₂ VCDs from relative differences of the GEMS IUP-UB NO₂ product (blue, light blue) and at the individual ground-based stations (red, light red) sites for weekdays (Monday-Friday) the different seasons. Stations are color-coded. The median, respectively weekends (Saturday and Sunday) including differences of all stations, is shown as black bars. Error bars represent the 25 and 75% quantiles of the MAX-DOAS and GEMS observations. Station names Results are only included if more than 20 observations are available per time bin and measurement periods can be found in the individual titles station.

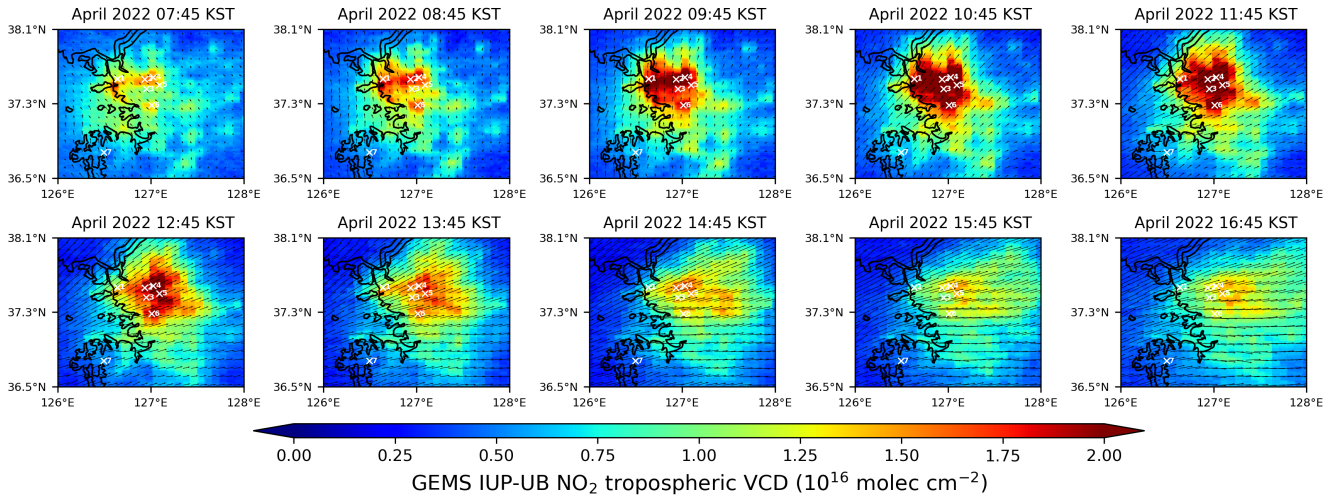


Figure A10. Maps of GEMS IUP-UB tropospheric NO₂ VCDs for the ten observations per day averaged for April 2022 overlaid with ERA5 10 m wind data. Arrow lengths indicate wind speed, and their orientation represents wind direction. Maps show the SMA, including the sites of the MAX-DOAS IUP-UB Incheon (1), Pandora Yonsei (2), Pandora Seoul (3), MAX-DOAS BIRA Seoul (4), MAX-DOAS MPIC Seoul (5), MAX-DOAS BIRA Suwon (6), and Pandora Seosan (7).

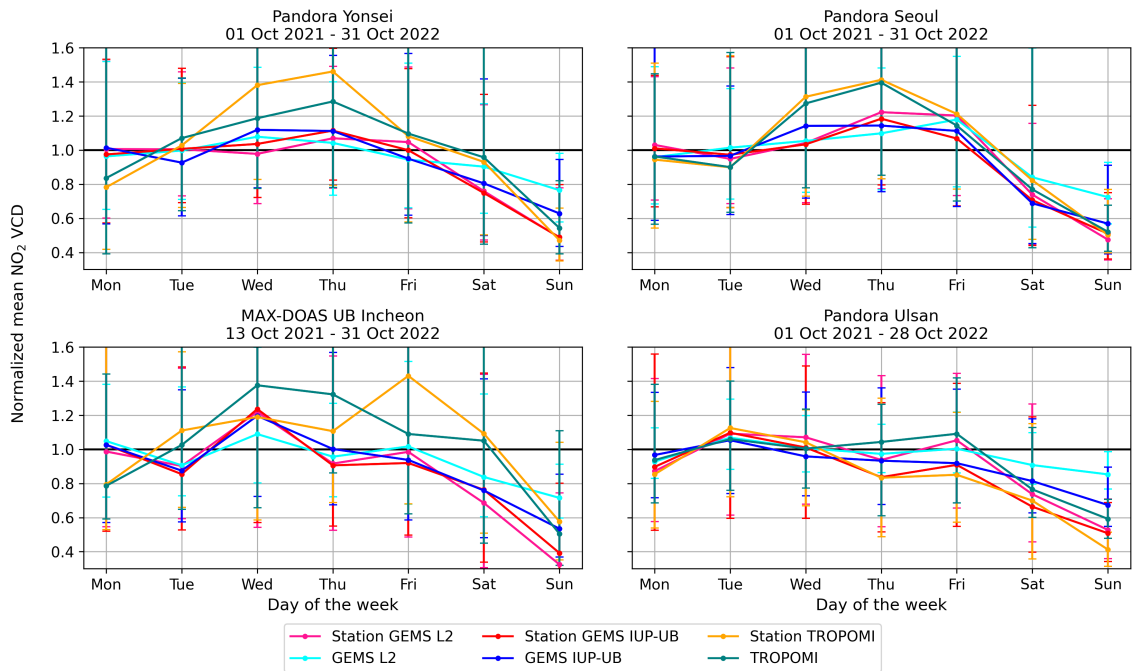


Figure A11. Remaining sites not shown in Fig. 11. Plots of normalized weekday NO₂ VCDs for the co-located station observations with the GEMS IUP-UB, the GEMS L2, and the TROPOMI observations.

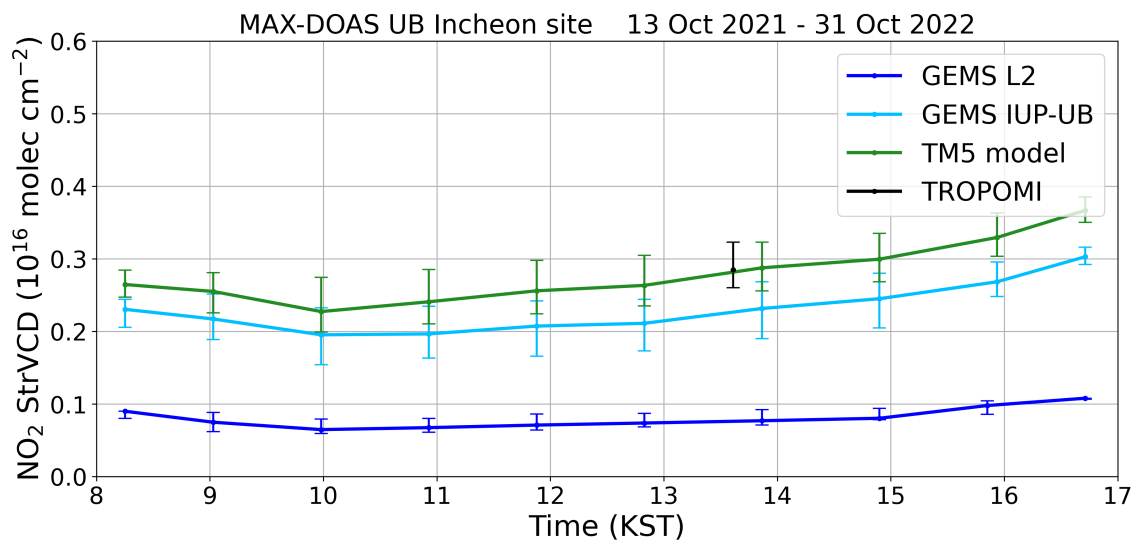


Figure A12. Diurnal variation of median stratospheric NO_2 VCDs for the GEMS L2 product based on the method from Bucselá et al. (2013) in dark blue, the GEMS IUP-UB STREAM-based product in light blue, and in green the TM5 model stratospheric VCDs, used for the TROPOMI product, which is shown in black.

References

- Beirle, S., Platt, U., Wenig, M., and Wagner, T.: Weekly cycle of NO₂ by GOME measurements: a signature of anthropogenic sources, *Atmospheric Chemistry and Physics*, 3, 2225–2232, <https://doi.org/10.5194/acp-3-2225-2003>, 2003.
- 820 Beirle, S., Boersma, K. F., Platt, U., Lawrence, M. G., and Wagner, T.: Megacity emissions and lifetimes of nitrogen oxides probed from space, *Science*, 333, 1737–1739, <https://doi.org/10.1126/science.1207824>, 2011.
- Beirle, S., Hörmann, C., Jöckel, P., Liu, S., Penning de Vries, M., Pozzer, A., Sihler, H., Valks, P., and Wagner, T.: The STRatospheric Estimation Algorithm from Mainz (STREAM): estimating stratospheric NO₂ from nadir-viewing satellites by weighted convolution, *Atmospheric Measurement Techniques*, 9, 2753–2779, <https://doi.org/10.5194/amt-9-2753-2016>, 2016.
- 825 Beirle, S., Borger, C., Dörner, S., Li, A., Hu, Z., Liu, F., Wang, Y., and Wagner, T.: Pinpointing nitrogen oxide emissions from space, *Science advances*, 5, eaax9800, <https://doi.org/10.1126/sciadv.aax9800>, 2019a.
- Beirle, S., Dörner, S., Donner, S., Remmers, J., Wang, Y., and Wagner, T.: The Mainz profile algorithm (MAPA), *Atmospheric Measurement Techniques*, 12, 1785–1806, <https://doi.org/10.5194/amt-12-1785-2019>, 2019b.
- Boersma, K. F., Jacob, D. J., Eskes, H. J., Pinder, R. W., Wang, J., and van der A, R. J.: Intercomparison of SCIAMACHY and OMI tropospheric NO₂ columns: Observing the diurnal evolution of chemistry and emissions from space, *Journal of Geophysical Research: Atmospheres*, 113, <https://doi.org/10.1029/2007jd008816>, 2008.
- 830 Boersma, K. F., Jacob, D. J., Trainic, M., Rudich, Y., DeSmedt, I., Dirksen, R., and Eskes, H. J.: Validation of urban NO₂ concentrations and their diurnal and seasonal variations observed from the SCIAMACHY and OMI sensors using in situ surface measurements in Israeli cities, *Atmospheric Chemistry and Physics*, 9, 3867–3879, <https://doi.org/10.5194/acp-9-3867-2009>, 2009.
- Bovensmann, H., Burrows, J., Buchwitz, M., Frerick, J., Noël, S., Rozanov, V., Chance, K., and Goede, A.: SCIAMACHY: Mission objectives and measurement modes, *Journal of the atmospheric sciences*, 56, 127–150, 1999.
- 835 Bucsela, E. J., Krotkov, N. A., Celarier, E. A., Lamsal, L. N., Swartz, W. H., Bhartia, P. K., Boersma, K. F., Veefkind, J. P., Gleason, J. F., and Pickering, K. E.: A new stratospheric and tropospheric NO₂ retrieval algorithm for nadir-viewing satellite instruments: applications to OMI, *Atmospheric Measurement Techniques*, 6, 2607–2626, <https://doi.org/10.5194/amt-6-2607-2013>, 2013.
- Burrows, J., Bovensmann, H., Bergametti, G., Flaud, J., Orphal, J., Noël, S., Monks, P., Corlett, G., Goede, A., von Clarmann, T., Steck, T., 840 Fischer, H., and Friedl-Vallon, F.: The geostationary tropospheric pollution explorer (GeoTROPE) mission: objectives, requirements and mission concept, *Advances in Space Research*, 34, 682–687, <https://doi.org/10.1016/j.asr.2003.08.067>, 2004.
- Burrows, J. P., Weber, M., Buchwitz, M., Rozanov, V., Ladstätter-Weissenmayer, A., Richter, A., DeBeek, R., Hoogen, R., Bramstedt, K., Eichmann, K.-U., Eisinger, M., and Perner, D.: The Global Ozone Monitoring Experiment (GOME): Mission Concept and First Scientific Results, *Journal of the Atmospheric Sciences*, 56, 151 – 175, https://journals.ametsoc.org/view/journals/atsc/56/2/1520-0469_1999_056_0151_tgomeg_2.0.co_2.xml, 1999.
- 845 Cede, A.: Manual for Blick Software Suite 1.8, Tech. rep., last access: 24 January 2024, 2021.
- [Chong, H., Lee, H., Koo, J.-H., Kim, J., Jeong, U., Kim, W., Kim, S.-W., Herman, J. R., Abuhassan, N. K., Ahn, J.-Y., Park, J.-H., Kim, S.-K., Moon, K.-J., Choi, W.-J., and Park, S. S.: Regional Characteristics of NO₂ Column Densities from Pandora Observations during the MAPS-Seoul Campaign, *Aerosol and Air Quality Research*, 18, 2207–2219, <https://doi.org/10.4209/aaqr.2017.09.0341>, 2018.](https://doi.org/10.4209/aaqr.2017.09.0341)
- 850 Dimitropoulou, E., Hendrick, F., Pinardi, G., Friedrich, M. M., Merlaud, A., Tack, F., De Longueville, H., Fayt, C., Hermans, C., Laffineur, Q., Fierens, F., and Van Roozendaal, M.: Validation of TROPOMI tropospheric NO₂ columns using dual-scan multi-axis differential

- optical absorption spectroscopy (MAX-DOAS) measurements in Uccle, Brussels, *Atmospheric Measurement Techniques*, 13, 5165–5191, <https://doi.org/10.5194/amt-13-5165-2020>, 2020.
- 855 [Edwards, D. P., Martínez-Alonso, S., Jo, D. S., Ortega, I., Emmons, L. K., Orlando, J. J., Worden, H. M., Kim, J., Lee, H., Park, J., and Hong, H.: Quantifying the diurnal variation in atmospheric NO₂ from Geostationary Environment Monitoring Spectrometer \(GEMS\) observations, *Atmospheric Chemistry and Physics*, 24, 8943–8961, <https://doi.org/10.5194/acp-24-8943-2024>, 2024.](#)
- Eskes, H. and Eichmann, K.: S5P MPC Product Readme Nitrogen Dioxide, Tech. rep., last access: 14 December 2023, 2023.
- Faustini, A., Rapp, R., and Forastiere, F.: Nitrogen dioxide and mortality: review and meta-analysis of long-term studies, *European Respiratory Journal*, 44, 744–753, <https://doi.org/10.1183/09031936.00114713>, 2014.
- 860 Friedrich, M. M., Rivera, C., Stremme, W., Ojeda, Z., Arellano, J., Bezanilla, A., García-Reynoso, J. A., and Grutter, M.: NO₂ vertical profiles and column densities from MAX-DOAS measurements in Mexico City, *Atmospheric Measurement Techniques*, 12, 2545–2565, <https://doi.org/10.5194/amt-12-2545-2019>, 2019.
- Hendrick, F., Pinardi, G., Van Roozendael, M., Apituley, A., Pitters, A., Richter, A., Wagner, T., Kreher, K., Friess, U., and Lampel, J.: Fiducial Reference Measurements for Ground-Based DOAS Air-Quality Observations, Deliverable D13 ESA Contract No.4000118181/16/I-EF, https://firm4doas.aeronomie.be/ProjectDir/Deliverables/FRM4DOAS_D13_Campaign_Planning_Document_20161021_final.pdf, last access 14 July 2022, 2016.
- 865 Hendrick, F., Friedrich, M., Fayt, C., Bais, A., Beirle, S., Bösch, T., Navarro Comas, M., Friess, U., Kariagkiozidis, D., Merlaud, A., Pinardi, G., Pitters, A., Puentedura, O., Prados, C., Reischmann, L., Richter, A., Wagner, T., Ziegler, S., and Van Roozendael, M.: FRM4DOAS: A Fiducial Reference Measurements System for Air Quality monitoring using ground-based MAX-DOAS instruments, *Atmospheric Measurement Techniques*, in preparation, 2024.
- 870 Herman, J., Cede, A., Spinei, E., Mount, G., Tzortziou, M., and Abuhassan, N.: NO₂ column amounts from ground-based Pandora and MF-DOAS spectrometers using the direct-sun DOAS technique: Intercomparisons and application to OMI validation, *Journal of Geophysical Research: Atmospheres*, 114, <https://doi.org/10.1029/2009jd011848>, 2009.
- Hersbach, H., Bell, B., Berrisford, P., Biavati, G., Horányi, A., Muñoz Sabater, J., Nicolas, J., Peubey, C., Radu, R., Rozum, I., Schepers, D., 875 Simmons, A., Soci, C., Dee, D., and Thépaut, J.-N.: ERA5 hourly data on single levels from 1940 to present, Copernicus Climate Change Service (C3S) Climate Data Store (CDS), <https://doi.org/10.24381/cds.adbb2d47>, last access: 07 February 2024, 2023.
- Hönninger, G., von Friedeburg, C., and Platt, U.: Multi axis differential optical absorption spectroscopy (MAX-DOAS), *Atmospheric Chemistry and Physics*, 4, 231–254, <https://doi.org/10.5194/acp-4-231-2004>, 2004.
- Ingmann, P., Veihelmann, B., Langen, J., Lamarre, D., Stark, H., and Courrèges-Lacoste, G. B.: Requirements for the GMES 880 Atmosphere Service and ESA's implementation concept: Sentinels-4/-5 and -5p, *Remote Sensing of Environment*, 120, 58–69, <https://doi.org/https://doi.org/10.1016/j.rse.2012.01.023>, the Sentinel Missions - New Opportunities for Science, 2012.
- Kim, J., Jeong, U., Ahn, M.-H., Kim, J. H., Park, R. J., Lee, H., Song, C. H., Choi, Y.-S., Lee, K.-H., Yoo, J.-M., Jeong, M.-J., Park, S. K., Lee, K.-M., Song, C.-K., Kim, S.-W., Kim, Y. J., Kim, S.-W., Kim, M., Go, S., Liu, X., Chance, K., Miller, C. C., Al-Saadi, J., Veihelmann, B., Bhartia, P. K., Torres, O., Abad, G. G., Haffner, D. P., Ko, D. H., Lee, S. H., Woo, J.-H., Chong, H., Park, S. S., Nicks, D., Choi, W. J., 885 Moon, K.-J., Cho, A., Yoon, J., kyun Kim, S., Hong, H., Lee, K., Lee, H., Lee, S., Choi, M., Veefkind, P., Levelt, P. F., Edwards, D. P., Kang, M., Eo, M., Bak, J., Baek, K., Kwon, H.-A., Yang, J., Park, J., Han, K. M., Kim, B.-R., Shin, H.-W., Choi, H., Lee, E., Chong, J., Cha, Y., Koo, J.-H., Irie, H., Hayashida, S., Kasai, Y., Kanaya, Y., Liu, C., Lin, J., Crawford, J. H., Carmichael, G. R., Newchurch, M. J., Lefer, B. L., Herman, J. R., Swap, R. J., Lau, A. K. H., Kurosu, T. P., Jaross, G., Ahlers, B., Dobber, M., McElroy, C. T., and Choi, Y.:

- New Era of Air Quality Monitoring from Space: Geostationary Environment Monitoring Spectrometer (GEMS), *Bulletin of the American Meteorological Society*, 101, E1 – E22, <https://doi.org/10.1175/BAMS-D-18-0013.1>, 2020.
- 890 Kim, S., Kim, D., Hong, H., Chang, L.-S., Lee, H., Kim, D.-R., Kim, D., Yu, J.-A., Lee, D., Jeong, U., Song, C.-K., Kim, S.-W., Park, S. S., Kim, J., Hanisco, T. F., Park, J., Choi, W., and Lee, K.: First-time comparison between NO₂ vertical columns from Geostationary Environment Monitoring Spectrometer (GEMS) and Pandora measurements, *Atmospheric Measurement Techniques*, 16, 3959–3972, <https://doi.org/10.5194/amt-16-3959-2023>, 2023.
- 895 Lambert, J.-C., Keppens, A., Compernelle, S., Eichmann, K.-U., de Graaf, M., Hubert, D., Langerock, B., Ludewig, A., Sha, M., Verhoelst, T., Wagner, T., Ahn, C., Argyrouli, A., Balis, D., Chan, K., Coldewey-Egbers, M., Smedt, I. D., Eskes, H., Fjæraa, A., Garane, K., Gleason, J., Goutail, F., Granville, J., Hedelt, P., Ahn, C., Heue, K.-P., Jaross, G., Kleipool, Q., Koukouli, M., Lutz, R., Velarte, M. M., Michailidis, K., Nanda, S., Niemeijer, S., Pazmiño, A., Pinaridi, G., Richter, A., Rozemeijer, N., Sneep, M., Zweers, D. S., Theys, N., Tilstra, G., Torres, O., Valks, P., van Geffen, J., Vigouroux, C., Wang, P., , and Weber, M.: Quarterly Validation Report of the Copernicus Sentinel-5
- 900 Precursor Operational Data Products: April 2018 – November 2023, Tech. rep., last access: 29 February 2024, 2023.
- Lange, K., Richter, A., and Burrows, J. P.: Variability of nitrogen oxide emission fluxes and lifetimes estimated from Sentinel-5P TROPOMI observations, *Atmospheric Chemistry and Physics*, 22, 2745–2767, <https://doi.org/10.5194/acp-22-2745-2022>, 2022.
- Lange, K., Richter, A., Schönhardt, A., Meier, A. C., Bösch, T., Seyler, A., Krause, K., Behrens, L. K., Wittrock, F., Merlaud, A., Tack, F., Fayt, C., Friedrich, M. M., Dimitropoulou, E., Van Roozendael, M., Kumar, V., Donner, S., Dörner, S., Lauster, B., Razi, M., Borger, C., Uhlmannsieck, K., Wagner, T., Ruhtz, T., Eskes, H., Bohn, B., Santana Diaz, D., Abuhassan, N., Schüttemeyer, D., and Burrows, J. P.: Validation of Sentinel-5P TROPOMI tropospheric NO₂ products by comparison with NO₂ measurements from airborne imaging DOAS, ground-based stationary DOAS, and mobile car DOAS measurements during the S5P-VAL-DE-Ruhr campaign, *Atmospheric Measurement Techniques*, 16, 1357–1389, <https://doi.org/10.5194/amt-16-1357-2023>, 2023.
- 905 Lee, H., Park, J., and Hong, H.: Geostationary Environment Monitoring Spectrometer (GEMS), Algorithm Theoretical Basis Document, NO₂ Retrieval Algorithm, Tech. rep., Environmental Satellite Center, National Institute of Environmental Research, Ministry of Environment, Issue 1.1, available at <https://nesc.nier.go.kr/en/html/satellite/doc/doc.do>, last access: 23 February 2024, 2020.
- Levelt, P. F., van den Oord, G. H., Dobber, M. R., Malkki, A., Visser, H., de Vries, J., Stammes, P., Lundell, J. O., and Saari, H.: The ozone monitoring instrument, *IEEE Transactions on geoscience and remote sensing*, 44, 1093–1101, <https://doi.org/10.1109/TGRS.2006.872333>, 2006.
- 915 Lorente, A., Boersma, K., Eskes, H., Veefkind, J., Van Geffen, J., de Zeeuw, M., van der Gon, H. D., Beirle, S., and Krol, M.: Quantification of nitrogen oxides emissions from build-up of pollution over Paris with TROPOMI, *Scientific reports*, 9, 1–10, <https://doi.org/10.1038/s41598-019-56428-5>, 2019.
- Ma, J. Z., Beirle, S., Jin, J. L., Shaiganfar, R., Yan, P., and Wagner, T.: Tropospheric NO₂ vertical column densities over Beijing: results of the first three years of ground-based MAX-DOAS measurements (2008–2011) and satellite validation, *Atmospheric Chemistry and Physics*, 13, 1547–1567, <https://doi.org/10.5194/acp-13-1547-2013>, 2013.
- 920 Munro, R., Eisinger, M., Anderson, C., Callies, J., Corpaccioli, E., Lang, R., Lefebvre, A., Livschitz, Y., and Albinana, A. P.: GOME-2 on MetOp, in: Proc. of The 2006 EUMETSAT Meteorological Satellite Conference, Helsinki, Finland, vol. 1216, p. 48, 2006.
- [Oak, Y. J., Jacob, D. J., Balasus, N., Yang, L. H., Chong, H., Park, J., Lee, H., Lee, G. T., Ha, E. S., Park, R. J., Kwon, H.-A., and Kim, J.: A bias-corrected GEMS geostationary satellite product for nitrogen dioxide using machine learning to enforce consistency with the TROPOMI satellite instrument, *EGUsphere*, 2024, 1–19, <https://doi.org/10.5194/egusphere-2024-393>, 2024.](https://doi.org/10.5194/egusphere-2024-393)
- 925 Pandonia Global Network: PGN data archive [data set], <http://data.pandonia-global-network.org/>, last access: 4 February 2023.

- Penn, E. and Holloway, T.: Evaluating current satellite capability to observe diurnal change in nitrogen oxides in preparation for geostationary satellite missions, *Environmental Research Letters*, 15, 034038, <https://doi.org/10.1088/1748-9326/ab6b36>, 2020.
- 930 Pinardi, G., Van Roozendael, M., Hendrick, F., Theys, N., Abuhassan, N., Bais, A., Boersma, F., Cede, A., Chong, J., Donner, S., Drosoglou, T., Dzhola, A., Eskes, H., Frieß, U., Granville, J., Herman, J. R., Holla, R., Hovila, J., Irie, H., Kanaya, Y., Karagiozidis, D., Kouremeti, N., Lambert, J.-C., Ma, J., Peters, E., Piters, A., Postlyakov, O., Richter, A., Remmers, J., Takashima, H., Tiefengraber, M., Valks, P., Vlemmix, T., Wagner, T., and Wittrock, F.: Validation of tropospheric NO₂ column measurements of GOME-2A and OMI using MAX-DOAS and direct sun network observations, *Atmospheric Measurement Techniques*, 13, 6141–6174, <https://doi.org/10.5194/amt-13-6141-2020>, 2020.
- 935 Platt, U. and Perner, D.: Direct measurements of atmospheric CH₂O, HNO₂, O₃, NO₂, and SO₂ by differential optical absorption in the near UV, *Journal of Geophysical Research: Oceans*, 85, 7453–7458, <https://doi.org/10.1029/JC085iC12p07453>, 1980.
- Richter, A., Lange, K., Burrows, J., Bösch, H., Kim, S.-W., Seo, S., Kim, K.-M., Hong, H., Lee, H., and Park, J.: An improved tropospheric NO₂ retrieval for GEMS, *Atmospheric Measurement Techniques*, in preparation, 2024.
- 940 Rozanov, V., Rozanov, A., Kokhanovsky, A., and Burrows, J.: Radiative transfer through terrestrial atmosphere and ocean: Software package SCIATRAN, *Journal of Quantitative Spectroscopy and Radiative Transfer*, 133, 13–71, <https://doi.org/10.1016/j.jqsrt.2013.07.004>, 2014.
- Seinfeld, J. H. and Pandis, S. N.: *Atmospheric Chemistry and Physics*, John Wiley & Sons Inc., Hoboken, New Jersey, 2006.
- Sentinel-5P Pre-Operations Data Hub: Offline L2 NO₂ [data set], <https://s5phub.copernicus.eu/>, last access: 21 February 2022.
- 945 [Seo, S., Kim, S.-W., Kim, K.-M., Richter, A., Lange, K., Burrows, J. P., Park, J., Hong, H., Lee, H., Jeong, U., and Kim, J.: Diurnal variations of NO₂ tropospheric vertical column density over the Seoul Metropolitan Area from the Geostationary Environment Monitoring Spectrometer \(GEMS\): seasonal differences and impacts of varying *a priori* NO₂ profile data, *Atmospheric Measurement Techniques Discussions*, 2024, 1–28, <https://doi.org/10.5194/amt-2024-33>, 2024.](https://doi.org/10.5194/amt-2024-33)
- Souri, A. H., Kumar, R., Chong, H., Golbazi, M., Knowland, K. E., Geddes, J., and Johnson, M. S.: Decoupling in the vertical shape of HCHO during a sea breeze event: The effect on trace gas satellite retrievals and column-to-surface translation, *Atmospheric Environment*, 309, 119929, <https://doi.org/10.1016/j.atmosenv.2023.119929>, 2023.
- 950 Spurr, R. J.: VLIDORT: A linearized pseudo-spherical vector discrete ordinate radiative transfer code for forward model and retrieval studies in multilayer multiple scattering media, *Journal of Quantitative Spectroscopy and Radiative Transfer*, 102, 316–342, <https://doi.org/10.1016/j.jqsrt.2006.05.005>, 2006.
- Stavrakou, T., Müller, J.-F., Bauwens, M., Boersma, K., and van Geffen, J.: Satellite evidence for changes in the NO₂ weekly cycle over large cities, *Scientific reports*, 10, 1–9, <https://doi.org/10.1038/s41598-020-66891-0>, 2020.
- 955 Tilstra, L. G., de Graaf, M., Trees, V., Litvinov, P., Dubovik, O., and Stammes, P.: A directional surface reflectance climatology determined from TROPOMI observations, *Atmospheric Measurement Techniques Discussions*, 2023, 1–29, <https://doi.org/10.5194/amt-2023-222>, 2023.
- van der A, R. J., Eskes, H. J., Boersma, K. F., van Noije, T. P. C., Van Roozendael, M., De Smedt, I., Peters, D. H. M. U., and Meijer, E. W.: Trends, seasonal variability and dominant NO_x source derived from a ten year record of NO₂ measured from space, *Journal of Geophysical Research: Atmospheres*, 113, D04302, <https://doi.org/10.1029/2007JD009021>, 2008.
- 960 van Geffen, J., Eskes, H., Boersma, K., and Veefkind, J.: TROPOMI ATBD of the total and tropospheric NO₂ data products, Tech. rep., 5P-KNMI-L2-0005-RP, Issue 2.4.0, available at <https://sentinel.esa.int/documents/247904/2476257/sentinel-5p-tropomi-atbd-no2-data-products>, last access: 18 December 2022, 2022.

- 965 Veefkind, J., Aben, I., McMullan, K., Förster, H., de Vries, J., Otter, G., Claas, J., Eskes, H., de Haan, J., Kleipool, Q., van Weele, M., Hasekamp, O., Hoogeveen, R., Landgraf, J., Snel, R., Tol, P., Ingmann, P., Voors, R., Kruizinga, B., Vink, R., Visser, H., and Levelt, P.: TROPOMI on the ESA Sentinel-5 Precursor: A GMES mission for global observations of the atmospheric composition for climate, air quality and ozone layer applications, *Remote Sensing of Environment*, 120, 70–83, <https://doi.org/10.1016/j.rse.2011.09.027>, the Sentinel Missions - New Opportunities for Science, 2012.
- 970 Verhoelst, T., Compernelle, S., Pinardi, G., Lambert, J.-C., Eskes, H. J., Eichmann, K.-U., Fjæraa, A. M., Granville, J., Niemeijer, S., Cede, A., Tiefengraber, M., Hendrick, F., Pazmiño, A., Bais, A., Bazureau, A., Boersma, K. F., Bogner, K., Dehn, A., Donner, S., Elokho, A., Gebetsberger, M., Goutail, F., Grutter de la Mora, M., Gruzdev, A., Gratsea, M., Hansen, G. H., Irie, H., Jepsen, N., Kanaya, Y., Karagiozidis, D., Kivi, R., Kreher, K., Levelt, P. F., Liu, C., Müller, M., Navarro Comas, M., Piters, A. J. M., Pommereau, J.-P., Portafaix, T., Prados-Roman, C., Puentedura, O., Querel, R., Remmers, J., Richter, A., Rimmer, J., Rivera Cárdenas, C., Saavedra de Miguel, L., Sinyakov, V. P., Stremme, W., Strong, K., Van Roozendael, M., Veefkind, J. P., Wagner, T., Wittrock, F., Yela González, M., and Zehner, 975 C.: Ground-based validation of the Copernicus Sentinel-5P TROPOMI NO₂ measurements with the NDACC ZSL-DOAS, MAX-DOAS and Pandonia global networks, *Atmospheric Measurement Techniques*, 14, 481–510, <https://doi.org/10.5194/amt-14-481-2021>, 2021.
- Wagner, T., Ibrahim, O., Shaiganfar, R., and Platt, U.: Mobile MAX-DOAS observations of tropospheric trace gases, *Atmospheric Measurement Techniques*, 3, 129–140, <https://doi.org/10.5194/amt-3-129-2010>, 2010.
- Wallace, J. M. and Hobbs, P. V.: *Atmospheric science: an introductory survey*, vol. 92, Elsevier, https://www.ebook.de/de/product/4444872/john_m_university_of_washington_seattle_u_s_a_wallace_peter_v_university_of_washington_seattle_u_s_a_hobbs_atmospheric_science.html, 2006.
- 980 Williams, J. E., Boersma, K. F., Le Sager, P., and Verstraeten, W. W.: The high-resolution version of TM5-MP for optimized satellite retrievals: description and validation, *Geoscientific Model Development*, 10, 721–750, <https://doi.org/10.5194/gmd-10-721-2017>, 2017.
- Wittrock, F., Oetjen, H., Richter, A., Fietkau, S., Medeke, T., Rozanov, A., and Burrows, J. P.: MAX-DOAS measurements of atmospheric trace gases in Ny-Ålesund - Radiative transfer studies and their application, *Atmospheric Chemistry and Physics*, 4, 955–966, 985 <https://doi.org/10.5194/acp-4-955-2004>, 2004.
- Xu, T., Zhang, C., Xue, J., Hu, Q., Xing, C., and Liu, C.: Estimating Hourly Nitrogen Oxide Emissions over East Asia from Geostationary Satellite Measurements, *Environmental Science & Technology Letters*, <https://doi.org/10.1021/acs.estlett.3c00467>, 2023.
- 990 Yang, L. H., Jacob, D. J., Colombi, N. K., Zhai, S., Bates, K. H., Shah, V., Beaudry, E., Yantosca, R. M., Lin, H., Brewer, J. F., Chong, H., Travis, K. R., Crawford, J. H., Lamsal, L. N., Koo, J.-H., and Kim, J.: Tropospheric NO₂ vertical profiles over South Korea and their relation to oxidant chemistry: implications for geostationary satellite retrievals and the observation of NO₂ diurnal variation from space, *Atmospheric Chemistry and Physics*, 23, 2465–2481, <https://doi.org/10.5194/acp-23-2465-2023>, 2023a.
- Yang, L. H., Jacob, D. J., Dang, R., Oak, Y. J., Lin, H., Kim, J., Zhai, S., Colombi, N. K., Pendergrass, D. C., Beaudry, E., Shah, V., Feng, 995 X., Yantosca, R. M., Chong, H., Park, J., Lee, H., Lee, W.-J., Kim, S., Kim, E., Travis, K. R., Crawford, J. H., and Liao, H.: Interpreting [GEMS Geostationary Environment Monitoring Spectrometer \(GEMS\)](https://doi.org/10.5194/acp-24-7027-2024) geostationary satellite observations of the diurnal variation of in nitrogen dioxide (NO₂) over East Asia, *EGU sphere*, 2023, 1–25, 2023. [Atmospheric Chemistry and Physics](https://doi.org/10.5194/acp-24-7027-2024), 24, 7027–7039, <https://doi.org/10.5194/acp-24-7027-2024>, 2024.

- 1000 Yang, Q., Kim, J., Cho, Y., Lee, W.-J., Lee, D.-W., Yuan, Q., Wang, F., Zhou, C., Zhang, X., Xiao, X., Guo, M., Guo, Y., Carmichael, G. R., and Gao, M.: A synchronized estimation of hourly surface concentrations of six criteria air pollutants with GEMS data, *npj Climate and Atmospheric Science*, 6, <https://doi.org/10.1038/s41612-023-00407-1>, 2023b.
- Zhang, Y., Lin, J., Kim, J., Lee, H., Park, J., Hong, H., Van Roozendaal, M., Hendrick, F., Wang, T., Wang, P., He, Q., Qin, K., Choi, Y., Kanaya, Y., Xu, J., Xie, P., Tian, X., Zhang, S., Wang, S., Cheng, S., Cheng, X., Ma, J., Wagner, T., Spurr, R., Chen, L., Kong, H.,
1005 and Liu, M.: A research product for tropospheric NO₂ columns from Geostationary Environment Monitoring Spectrometer based on Peking University OMI NO₂ algorithm, *Atmospheric Measurement Techniques*, 16, 4643–4665, <https://doi.org/10.5194/amt-16-4643-2023>, 2023.
- Zoogman, P., Liu, X., Suleiman, R., Pennington, W., Flittner, D., Al-Saadi, J., Hilton, B., Nicks, D., Newchurch, M., Carr, J., Janz, S., Andraschko, M., Arola, A., Baker, B., Canova, B., Chan Miller, C., Cohen, R., Davis, J., Dussault, M., Edwards, D., Fishman, J., Ghulam, A., González Abad, G., Grutter, M., Herman, J., Houck, J., Jacob, D., Joiner, J., Kerridge, B., Kim, J., Krotkov, N., Lamsal, L.,
1010 Li, C., Lindfors, A., Martin, R., McElroy, C., McLinden, C., Natraj, V., Neil, D., Nowlan, C., O’Sullivan, E., Palmer, P., Pierce, R., Pippin, M., Saiz-Lopez, A., Spurr, R., Szykman, J., Torres, O., Veefkind, J., Veihelmann, B., Wang, H., Wang, J., and Chance, K.: Tropospheric emissions: Monitoring of pollution (TEMPO), *Journal of Quantitative Spectroscopy and Radiative Transfer*, 186, 17–39, <https://doi.org/https://doi.org/10.1016/j.jqsrt.2016.05.008>, satellite Remote Sensing and Spectroscopy: Joint ACE-Odin Meeting, October
1015 2015, 2017.